Barley *Ror1* encodes a class XI myosin required for *mlo*-based broad-spectrum resistance to the fungal powdery mildew pathogen

Johanna Acevedo-Garcia[1,2,†,‡], Kim Walden[1,†], Franz Leissing[1], Kira Baumgarten[1], Katarzyna Drwiega[1], Mark Kwaaitaal[1], Anja Reinstädler[1], Matthias Freh[1], Xue Dong[3], Geo Velikkakam James[3,§], Lisa C. Baus[4], Martin Mascher[5], Nils Stein[5,6], Korbinian Schneeberger[3,4,7], Nahal Brocke-Ahmadinejad[8,9,¶], Martin Kollmar[10], Paul Schulze-Lefert[2] and Ralph Panstruga[1,2,*]

[1]Unit of Plant Molecular Cell Biology, Institute for Biology I, RWTH Aachen University, Worringerweg 1, 52056 Aachen, Germany,
[2]Department of Plant-Microbe Interactions, Max Planck Institute for Plant Breeding Research, Carl-von-Linné-Weg 10, 50829 Cologne, Germany,
[3]Department of Plant Developmental Biology, Max Planck Institute for Plant Breeding Research, Carl-von-Linné-Weg 10, 50829 Cologne, Germany,
[4]Faculty of Biology, LMU Munich, 82152 Planegg-Martinsried, Germany,
[5]Leibniz Institute of Plant Genetics and Crop Plant Research (IPK), Corrensstr. 3, 06466 Seeland, Germany,
[6]Center of integrated Breeding Research (CiBreed), Department of Crop Sciences, Georg-August-University Göttingen, Von Siebold Str. 8, 37075 Göttingen, Germany,
[7]Department of Chromosome Biology, Max Planck Institute for Plant Breeding Research, Carl-von-Linné-Weg 10, 50829 Cologne, Germany,
[8]INRES Crop Bioinformatics, University of Bonn, Katzenburgweg 2, 53115 Bonn, Germany,
[9]Institute of Biochemistry and Molecular Biology, University of Bonn, Nussallee 11, D-53115 Bonn, Germany, and
[10]Department of NMR-based Structural Biology, Group Systems Biology of Motor Proteins, Max-Planck-Institute for Biophysical Chemistry, Am Fassberg 11, 37077 Göttingen, Germany

SUMMARY

Loss-of-function alleles of plant *MLO* genes confer broad-spectrum resistance to powdery mildews in many eudicot and monocot species. Although barley (*Hordeum vulgare*) *mlo* mutants have been used in agriculture for more than 40 years, understanding of the molecular principles underlying this type of disease resistance remains fragmentary. Forward genetic screens in barley have revealed mutations in two *Required for mlo resistance* (*Ror*) genes that partially impair immunity conferred by *mlo* mutants. While *Ror2* encodes a soluble *N*-ethylmaleimide-sensitive factor-attached protein receptor (SNARE), the identity of *Ror1*, located at the pericentromeric region of barley chromosome 1H, remained elusive. We report the identification of *Ror1* based on combined barley genomic sequence information and transcriptomic data from *ror1* mutant plants. *Ror1* encodes the barley class XI myosin Myo11A (HORVU.MOREX.r3.1HG0046420). Single amino acid substitutions of this myosin, deduced from non-functional *ror1* mutant alleles, map to the nucleotide-binding region and the interface between the relay-helix and the converter domain of the motor protein. Ror1 myosin accumulates transiently in the course of powdery mildew infection. Functional fluorophore-labeled Ror1 variants associate with mobile intracellular compartments that partially colocalize with peroxisomes. Single-cell expression of the Ror1 tail region causes a dominant-negative effect that phenocopies *ror1* loss-of-function mutants. We define a myosin motor for the establishment of *mlo*-mediated resistance, suggesting that motor protein-driven intracellular transport processes are critical for extracellular immunity, possibly through the targeted transfer of antifungal and/or cell wall cargoes to pathogen contact sites.

Keywords: barley, *Hordeum vulgare*, *mlo* resistance, myosin XI, powdery mildew, suppressor mutant, *Blumeria hordei*.

INTRODUCTION

Powdery mildew is a common and widespread plant disease in temperate climates. It is caused by obligate biotrophic fungi, which taxonomically belong to the ascomycetes (order Helotiales, family Erysiphaceae). More than 10 000 angiosperm plant species are hosts of powdery mildew fungi and can be successfully colonized by the fungal phytopathogens (Glawe, 2008). Control of the disease can be achieved either by fungicides or genetically *via* the cultivation of resistant cultivars. Loss-of-function mutations in particular members of the plant *Mildew locus o* (*Mlo*) gene family, encoding heptahelical plant membrane proteins operating as 'susceptibility factors', result in highly effective immunity against powdery mildew infection (Kusch & Panstruga, 2017). Resistance conferred by the respective *mlo* mutants is effective at the stage of host cell entry and has been proven to be broad-spectrum (covering all genetic variants of a mildew species that is generally virulent on a given plant species) and remarkably durable. This type of recessively inherited disease resistance was first described in the case of barley *(Hordeum vulgare)* and its powdery mildew pathogen *Blumeria graminis* f.sp. *hordei* (reviewed in Jørgensen, 1992), which has been recently renamed *Blumeria hordei* (Liu et al., 2021). Natural and induced barley *mlo* mutants have been successfully used in European agriculture since the late 1970s (Lyngkjær et al., 2000). More recently, powdery mildew-resistant *mlo* mutants were described in a range of monocotyledonous and dicotyledonous plant species, including the reference plant *Arabidopsis thaliana* and important crops such as tomato (*Solanum lycopersicum*), pea (*Pisum sativum*), and wheat (*Triticum aestivum*), indicating that this type of immunity is conserved within the plant kingdom (Acevedo-Garcia, Spencer, et al., 2017; Bai et al., 2008; Consonni et al., 2006; Humphry et al., 2011; Wang et al., 2014). While *mlo* mutants arguably exert the most dramatic effect in response to powdery mildew attack, they were reported to show (slightly) altered infection phenotypes to a range of different microbes. These comprise not only a variety of phytopathogens (Acevedo-Garcia, Gruner, et al., 2017; Jarosch et al., 1999; McGrann et al., 2014), but also fungal symbionts (Hilbert et al., 2020; Jacott et al., 2020).

While Mlo proteins were recently found to act as plant-specific calcium channels (Gao et al., 2022), the molecular basis of *mlo*-mediated resistance remains enigmatic (Kusch et al., 2017). Scanning *N*-glycosylation mutagenesis and Mlo-Lep fusion protein analysis demonstrated that barley Mlo has seven transmembrane helices and resides predominantly in the plasma membrane, with the N- and C-termini located extracellularly and intracellularly, respectively (Devoto et al., 1999). The C-terminal cytoplasmic tail harbors a calmodulin-binding domain, and association of calmodulin to this region is required for full susceptibility to the pathogenic fungus (Kim et al., 2002). Pathogen attack triggers Mlo relocalization in single attacked leaf epidermal cells and results in focal accumulation beneath *B. hordei* contact sites (Bhat et al., 2005). Several of its amino acids are known to be critical for Mlo stability and function. Their mutational substitution results in unstable and/or non-functional Mlo protein variants (Elliott et al., 2005; Müller et al., 2005; Reinstädler et al., 2010).

A genetic screen in the background of the highly resistant barley *mlo*-5 null mutant genotype, conducted to identify genes that contribute to the *mlo* resistance phenotype, resulted in the isolation of mutant barley plants with partially restored *B. hordei* susceptibility. These chemically induced suppressor mutants, *required for mlo resistance* (*ror*), were mapped to two unlinked loci, designated *Ror1* and *Ror2* (Freialdenhoven et al., 1996). In the respective *mlo*-5 *ror* double mutants, not only is *mlo*-mediated resistance to *B. hordei* partially compromised, but also an associated pathogen-triggered burst of reactive oxygen species (ROS) is attenuated (Piffanelli et al., 2002). Notably, this effect of the *ror* mutations is specific for *mlo*-based broad-spectrum resistance and, thus, does not interfere with isolate-specific immunity to *B. hordei*, which is tightly linked to the activation of a hypersensitive cell death response at sites of attempted pathogen ingress (Peterhänsel et al., 1997).

Map-based cloning of *Ror2* revealed that the gene encodes a soluble *N*-ethylmaleimide (NEM)-sensitive factor-attached protein receptor (SNARE) (Collins et al., 2003). Ror2 resides at the plasma membrane and serves as a target membrane SNARE (t-SNARE) in vesicle fusion events by forming a ternary SNARE complex with its partner SNARE proteins, SNAP34 and VAMP721 (Kwaai-taal et al., 2010; Kwon et al., 2008). *Ror1*, located in the pericentromeric region of the long arm of barley chromosome 1H, proved recalcitrant to map-based cloning efforts. The corresponding genomic target region shows a low frequency of meiotic recombination events and a disruption in barley–rice (*Oryza sativa*) collinear gene order (synteny) (Collins et al., 2001). Later attempts to bridge the corresponding interval physically with the help of yeast artificial

chromosomes (YACs), which have large insertions of several hundred kb, led to the identification of new *Ror1*-flanking genes, but again failed to identify *Ror1* (Acevedo-Garcia et al., 2014).

Myosins form a superfamily of eukaryotic motor proteins that move along actin cytoskeleton tracks. They convert chemical energy in the form of adenosine triphosphate (ATP) into mechanical energy by coupling ATP hydrolysis to conformational changes that result in protein movement toward the plus end of actin filaments (Robert-Paganin et al., 2020). Myosins are probably best known for their role in human skeletal muscle. In plants, together with kinesins, which represent the other large group of plant motor proteins (associating with microtubules), they bind to different types of cellular cargo, enabling intracellular transport processes (Nebenführ & Dixit, 2018). Based on sequence similarity within the motor domain, myosins can be grouped into various classes (Kollmar & Mühlhausen, 2017), of which myosin VIII and myosin XI are the sole types present in plants (Mühlhausen & Kollmar, 2013). Class VIII and class XI myosins differ in domain organization, molecular mass, and kinetic properties (Nebenführ & Dixit, 2018). While the cellular functions of class VIII myosins remain largely elusive, several class XI myosins have been assigned isoform-specific tasks in intracellular movement of organelles through processive walking on actin filaments (Madison & Nebenführ, 2013; Ryan & Nebenführ, 2018; Tominaga et al., 2003).

Here, we describe the isolation of barley *Ror1* as a myosin XI-encoding gene. Using a series of seven independent mutant alleles and data from the analysis of barley recombinants we found that barley *HORVU.MOREX.r3. 1HG0046420*, encoding HvMyo11A1, is *Ror1*. By transient single-cell gene expression analysis, we demonstrate complementation of *mlo ror* double mutants by *Ror* and reveal a dominant-negative effect upon overexpression of the Ror1 tail region. The protein, which accumulates transiently in the course of the barley–powdery mildew interaction, is partially colocalized with peroxisomes, suggesting that the locomotion of these organelles and/or other endomembrane compartments is critical for extracellular defense in barley.

RESULTS

Positioning *Ror1*-flanking markers in the barley genome assembly

We pursued the identification of *Ror1* based on a still fragmented barley genome assembly of cultivar (cv.) Morex available from 2015 onwards. At that time, the genome assembly relied mainly on bacterial artificial chromosome (BAC) clusters (groups of overlapping BAC clones) that form a minimal tiling path for each chromosome. These

BACs were ordered using several approaches, including physical map information, genetic linkage, an optical map, and chromosome conformation capture sequencing (Hi-C). The advantage of Hi-C over genetic mapping is that the order of BAC clusters can also be resolved in pericentromeric regions where there is hardly any meiotic recombination. The Hi-C map assigned each BAC cluster to a consecutive position (a 'bin') along the chromosome (Mascher et al., 2017).

We performed BLAST (Altschul et al., 1990) searches using the previously identified *Ror1*-flanking genes as queries to determine their relative position within the Hi-C-based barley genome assembly. Most of these genes (*Ltp, Myo, Ppr, Pol, Mat, Noc, Con, Dep, Unk, Oxp*) were located in bins 205–211 in the pericentromeric region of chromosome 1H within an assumed interval of approximately 12 Mb (Table S1). The linear order of these genes within these bins was largely consistent with the deduced order established by our former work (Acevedo-Garcia et al., 2013). Two of the previously identified *Ror1*-flanking genes, *Smc* and *Far*, did not provide convincing BLAST hits, suggesting that these two genes are either absent from cv. Morex or not represented by the available BAC sequences. Indeed, the updated barley genome assembly (cv. Morex V3; Mascher et al., 2021) revealed that *Smc* is present in two near-identical copies, one located on chromosome 1H (*HORVU.MOREX.r3.1HG0095290*) at some distance from the *Ror1* target region and one located on chromosome 7H (*HORVU.MOREX.r3.7HG0697740*), suggesting that its presence on a YAC in our previous study was likely due to a chimeric clone. Additionally, an updated BLAST search showed that the sequence stretch previously designated as *Far*, originally thought to be part of a transcription factor gene, is actually a highly repetitive sequence, derived from *Sabrina*-like retrotransposons, present throughout the barley genome in dozens of near-identical copies.

A closer inspection of the gene order in the Hi-C map-based target interval revealed that a group of co-segregating genes flanking *Ror1* on the centromeric side appear to have undergone an inversion event in barley relative to the rice genome, which was formerly used as a template for marker order exploiting barley–rice synteny (Acevedo-Garcia et al., 2013; Collins et al., 2001). This finding positioned the previously closest *Ror1*-flanking gene on the centromeric side (*Pol*, AK375542, MLOC_15664, now *HORVU.MOREX.r3.1HG0045780*) further away from *Ror1*, making gene AK250464 (MLOC_1587.2, now *HORVU.MOR-EX.r3.1HG0046150*; encoding an α-galactosidase) the closest known marker centromeric of *Ror1* (Table S1, Figure 1). The nearest flanking genes on either side of *Ror1*, AK250464 (*HORVU.MOREX.r3.1HG0046150*, centromeric to *Ror1*) and AK371545 (*HORVU.MOREX.r3.1HG0046850*, *Con*, telomeric to *Ror1*), were located on two adjacent BAC
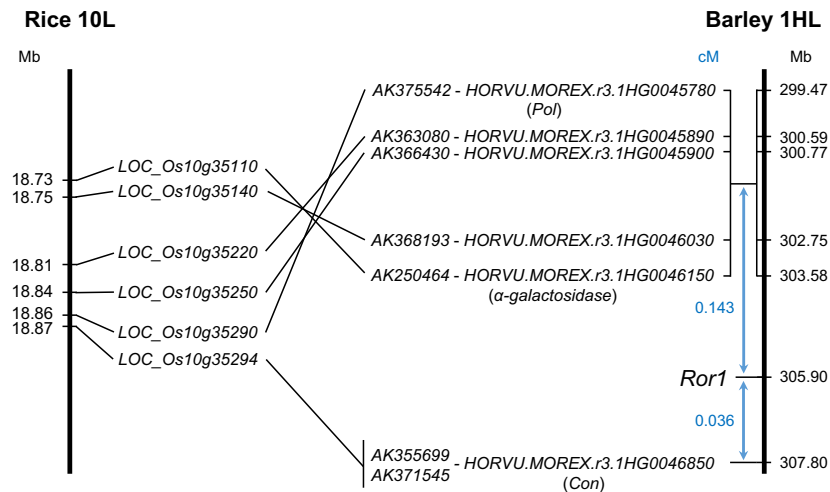
Figure 1. Inversion of a group of *Ror1*-flanking genes in barley relative to rice. Based on the barley Hi-C BAC cluster, a group of five barley genes (*AK375542*, *AK366430*, *AK363080*, *AK368193*, *AK250464*), residing on barley chromosome 1HL and co-segregating in genetic analysis in relation to *Ror1* at a genetic distance of 0.143 cM (blue font), was found to exhibit the opposite orientation to the respective rice orthologs on rice chromosome 10L. In contrast to previous belief, this renders gene *AK250464* (*HORVuHr1G043820*) the closest genetically mapped marker on the centromeric side of *Ror1*. The approximate locations and distances (in Mb) of the genes in the genomes of rice (*O. sativa* ssp. *japonica*; IRSGP1.0) and *H. vulgare* (MorexV3_pseudomolecules_assembly) are given according to EnsemblPlants (Release 52). Gene positions relate to the beginning of the respective genes as annotated in EnsemblPlants. Genetic distances (blue font) are based on Acevedo-Garcia et al. (2013).

clusters (86 and 193) of the barley cv. Morex assembly, corresponding to Hi-C bins 208 and 209. Assuming no errors in the Hi-C assembly or genetic map, we reasoned that the *Ror1* gene must be located either on these two clusters or in the gap between them. Based on optical map data, the space between the two adjacent BAC clusters was estimated to be below 180 kb in size. The known interval between *HORVU.MOREX.r3.1HG0046150* (α-galactosidase) and *HORVU.MOREX.r3.1HG0046850* (*Con*) included a total of 50 annotated genes, of which 26 were assigned as high-confidence (HC) and 24 as low-confidence (LC) genes (Table S1).

Identification of a *Ror1* candidate gene by whole-transcriptome shotgun sequencing (RNA-Seq) of barley *mlo*-5 *ror1* double mutants

We next aimed to identify *Ror1* by comparative RNA-Seq analysis of six of the seven chemically induced *mlo*-5 *ror1* double mutants (note that seed stocks of mutant *mlo*-5 *ror1*-6 were limited, and this genotype was therefore omitted from the RNA-Seq experiment) in comparison to the parental back-cross (BC) Ingrid *mlo*-5 line (*mlo Ror* genotype). We collected leaf material of the six *mlo*-5 *ror1* double mutants at 0, 6, and 18 h post-inoculation (hpi) with *B. hordei* conidiospores. Samples from two different *ror1* mutants were collected per time point, and a pool of leaves from the three time points was sampled for the mock-inoculated line BC Ingrid *mlo*-5 (Table S2). The leaf samples were used for RNA extraction, and total RNA was subjected to RNA-Seq analysis.

We mapped the resulting RNA-Seq reads of all genotypes against the original BAC assemblies for the BACs in the target interval. We noted the occurrence of putative mutational events (mostly single-nucleotide polymorphisms – see below) in several *mlo*-5 *ror1* double mutants in *MLOC_19838* and *MLOC_52235* genes, both of which were annotated as putative *myosin XI* genes. Closer inspection of these sequences revealed that they likely belong to the same *myosin XI* gene, with *MLOC_19838* representing the proximal half (encoding amino acids 11–557 relative to *Brachypodium distachyon* gene *Bradi3g29700.1*) and *MLOC_52235* representing the distal half (encoding amino acids 632–1219 relative to *Bradi3g29700.1*). We assembled the complete *myosin XI* candidate gene based on the combined sequences of *MLOC_19838* and *MLOC_52235*, supplemented by available sequence information of barley BAC clone HVVMRXALL-MA0296A07, which contains both *MLOC_19838* and *MLOC_52235* (Data S1). The resulting genomic sequence, which originates from cv. Morex, covers approximately 30 kb. The available RNA-Seq reads (Tables S2 and S3) allowed us to resolve the complex exon–intron structure of the candidate *myosin XI* gene (Figure 2a). It consists of 39 exons with a coding sequence of 4530 bp (including the stop codon; Data S1) and encodes a predicted protein of 1509 amino acids (Data S1) with a calculated molecular mass of 172.1 kDa. In the recently improved MorexV3_pseudo-molecules_assembly of cv. Morex (Mascher et al., 2021), accessible *via* EnsemblPlants (https://plants.ensembl.org/index.html; Release 52), this gene has since been given the designation *HORVU.MOREX.r3.1HG0046420* and the

encoded protein is designated *Hv*Myo11A1 (Figure S1). According to the EoRNA Barley Expression Database (https://ics.hutton.ac.uk/eorna/index.html), at least 26 different transcript forms (splice variants) of this gene exist.

Based on the full-length genome and cDNA sequences and manual reinspection of the RNA-Seq data, we identified detrimental mutational events in each of the seven *mlo*-5 *ror1* double mutants in gene *HORVU.MOREX.r3.1HG0046420*. We found that the coding sequence was identical between the Morex and Ingrid cultivars, while the covered intronic sequences revealed few cultivar-specific nucleotide differences. In six of the seven mutants, we found single-nucleotide substitutions in the *HORVU.MOREX.r3.1HG0046420* coding sequence, two of which are likely to result in an amino acid substitution (missense mutation; *mlo*-5 *ror1*-1 and *mlo*-5 *ror1*-2). Four other nucleotide substitutions affect consensus intron splice sites, resulting in predicted mis-splicing and, consequently, frame-shift mutations leading to premature stop codons (*mlo*-5 *ror1*-3, *mlo*-5 *ror1*-5, *mlo*-5 *ror1*-6, and *mlo*-5 *ror1*-7; Table 1). We noticed that the double mutants *mlo*-5 *ror1*-3 and *mlo*-5 *ror1*-5 had identical mutational events, affecting the same acceptor splice site at the end of intron 26. The seventh double mutant (*mlo*-5 *ror1*-4) is characterized by the near-complete absence of RNA-Seq reads in the *HORVU.MOREX.r3.1HG0046420* coding region (Table S3), suggesting a larger genomic deletion. We independently validated the detected point mutations and the absence of the transcript/genomic sequence (*mlo*-5 *ror1*-4) in the double mutants in comparison to the parental BC Ingrid *mlo*-5 single mutant by PCR and reverse transcription (RT)-PCR analysis in combination with Sanger sequencing of the respective amplicons (Figure S2).

To explore whether further mutational events are present in additional genes in the defined genetic target interval between *HORVU.MOREX.r3.1HG0046150* (α-galactosidase) and *HORVU.MOREX.r3.1HG0046850* (*Con*), we searched for mutational events based on the alignment of the RNA-Seq reads to the updated barley genome assembly (cv. Morex V3; Mascher et al., 2021). This led to the reidentification of the induced mutation in the *HORVU.MOREX.r3.1HG0046420 Ror1* candidate gene in the *mlo*-5 *ror1*-2 mutant but did not reveal any further mutational events in any of the neighboring genes in any of the mutant lines. The other mutations in *HORVU.MOREX.r3.1HG0046420* escaped detection by this analysis due to the absence of RNA-Seq reads (*mlo*-5 *ror1*-4), the lesions being located in intronic sequences not covered by the RNA-Seq reads (*mlo*-5 *ror1*-3, *mlo*-5 *ror1*-5, and *mlo*-5 *ror1*-7) or the low coverage by RNA-Seq reads in exons 1 to 14 in the case of the *mlo*-5 *ror1*-1 mutant. In sum, this analysis corroborates the identification of *HORVU.MOREX.r3.1HG0046420* as a candidate *Ror1* gene. It also demonstrates that there is no other gene with a detectable mutational event in coding sequences within the genetic target interval.

Marker analysis of barley recombinants within the *Ror1* genetic interval supports the identity of *HORVU.MOREX.r3.1HG0046420* as a candidate *Ror1* gene

We previously used a panel of 10 barley recombinants within the *Ror1* genetic interval to map candidate genes relative to *Ror1* (Acevedo-Garcia et al., 2013; Collins et al., 2001). These recombinants are based on crosses of line A89 (*mlo*-5 *ror1*-2 in the background of cv. Ingrid) and the *mlo*-3 mutant (*mlo*-3 *Ror1* genotype in the background of cv. Malteria Heda). The corresponding meiotic recombination events have been shown to be close to *Ror1* (Collins et al., 2001). We comparatively analyzed the *HORVU.MOREX.r3.1HG0046420* gene sequence in cv. Ingrid and cv. Malteria Heda to identify nucleotide polymorphisms between the two genotypes. We identified three single-nucleotide polymorphisms in the genomic region at position chr1H: 321583554 (G/C), chr1H: 321583601 (T/C), and chr1H: 321583629 (T/C), which could be used to determine the haplotype for the *HORVU.MOREX.r3.1HG0046420* candidate gene in the barley recombinants. Amplicon sequencing of the respective gene segments from eight of the recombinant lines revealed a haplotype pattern that is consistent with the expected *Ror1* genotype based on powdery mildew pathotype data (Figure S3).

Figure 2. *Hv*Myo11A1 gene/protein organization and phylogeny of plant myosins. (a) Exon–intron organization of *Hv*Myo11A1 (*HORVU.MOREX.r3.1HG0046420*) according to EnsemblPlants (Release 52), established with Exon-Intron Graphic Marker (http://wormweb.org/exonintron). The white rectangle on the left represents the 5′ untranslated region (5′ UTR), the white arrowhead on the right the represents the 3′ untranslated region (3′ UTR). Black rectangles signify exons, the connecting lines signify introns. Mutation sites are indicated by black triangles. The scale bar above the scheme equals 5000 bp. (b) Domain organization of the *Hv*Myo11A1 protein. The scheme illustrates the order and size of major protein domains within the *Hv*Myo11A1 myosin. Protein domains were identified with InterPro (https://www.ebi.ac.uk/interpro/) and the cartoon was established with IBS 1.0 (http://ibs.biocuckoo.org/). The scale bar above the cartoon equals 100 amino acids (aa). (c) Phylogeny of plant myosins. The unrooted maximum-likelihood tree shows the phylogeny of the myosin motor domains of the *A. thaliana* (At), *H. pubiflorum* (Hp), *H. vulgare* (Hv), and *O. sativa* ssp. *japonica* (Os_a) myosins. Branch support values (1000 bootstrap replicates) are provided for every node as percentages. Gene loci are indicated for the *A. thaliana*, *H. vulgare*, and *O. sativa* myosins as available at EnsemblPlants (Release 52). Please note that almost none of the gene structures currently presented at EnsemblPlants are correct and that only one gene 'locus' is given in case the correctly reconstructed gene spans multiple 'loci'. The correct sequences have been manually assembled and annotated (Kollmar & Mühlhausen, 2017) and are available at CyMoBase (https://www.cymobase.org/cymobase; Odronitz & Kollmar, 2007). Please note further that barley Myo1E4 (Figure S1) lacks a recognizable motor domain and, therefore, is not represented in this tree. The clade harboring Ror1 (*Hv*Myo11A1) is boxed in green. The previous nomenclature of the *A. thaliana* myosins is given for better orientation. The scale bar corresponds to estimated amino acid substitutions per site.

(a)

(b)

(c)
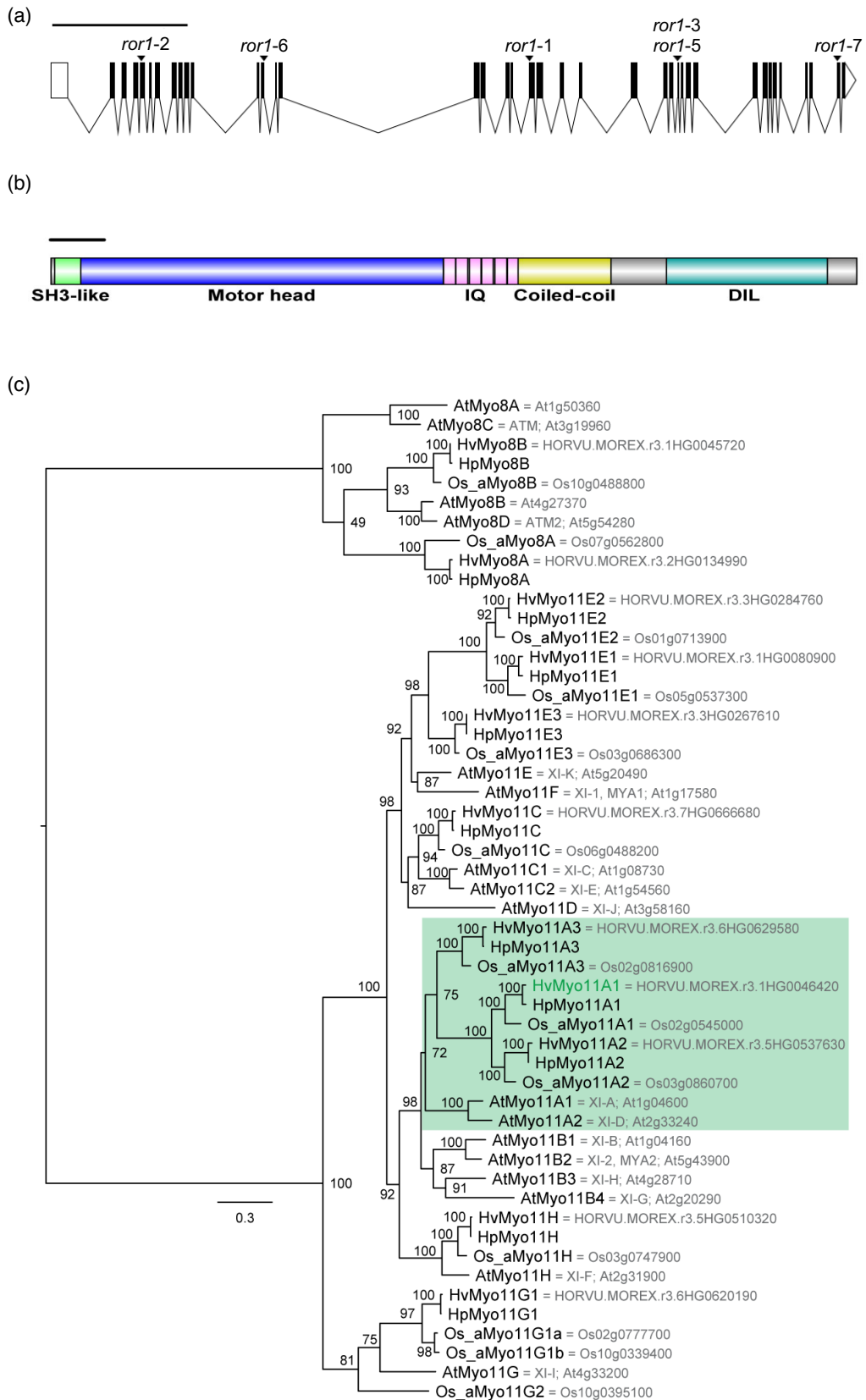
Ror1 is a presumptive co-ortholog of *A. thaliana* class XI myosins AtMyo11A1 (XI-A) and AtMyo11A2 (XI-D)

Similar to other class XI myosins, deduced Ror1 consists of an N-terminal SH3-like domain, a motor head, six calmodulin-binding IQ motifs forming the neck region, a coiled-coil region, and a C-terminal dilution (DIL) domain (Figure 2b). We constructed a phylogenetic tree of all barley, rice, and *A. thaliana* myosin proteins (Mühlhausen & Kollmar, 2013) based on the amino acid sequences of the motor domains, which due to its high degree of evolutionary conservation is the most informative region for phylogenetic inferences of myosins (Kollmar & Mühlhausen, 2017). This tree showed a clear separation of class VIII and class XI myosins and revealed a close association of Ror1 (HvMyo11A1) with two other barley myosin paralogs (HvMyo11A2 and HvMyo11A3) as putative co-orthologs of the two *A. thaliana* myosins AtMyo11A1 (XI-A) and AtMyo11A2 (XI-D) (Figure 2c). Similar to barley, the rice genome encodes three Myo11A paralogs (Os02g0545000, Os02g0816900, and Os03g0860700), of which, according to the phylogeny, Os02g0545000 seems to be the closest relative of Ror1. The branch containing Ror1 is a sister clade to a group that includes four other *A. thaliana* myosins – AtMyo11B1 (XI-B), AtMyo11B2 (XI-2), AtMyo11B3 (XI-H), and AtMyo11B4 (XI-G).

The *ror1-1* mutant encodes a stable non-functional mutant variant affected at the myosin relay-loop–converter interface

We expressed the proximal part of the C-terminal Ror1 tail domain (corresponding to amino acids 879–1509), which is a weakly conserved region among class XI myosins (Figure S4), in *Escherichia coli* and used the recombinant protein to raise a polyclonal α-Ror1 antiserum in rabbits. This antiserum recognizes an approximately 170-kDa protein in total cell lysates of pathogen-free barley primary leaves (wild-type plants; *Mlo Ror1* genotype; Figure 3). The deduced molecular mass agrees well with the calculated molecular mass of Ror1 (172.1 kDa). The antiserum detects an additional signal corresponding to approximately 110 kDa, which probably represents a natural or experimentally induced Ror1 cleavage product. Alternatively, this fragment could represent an N-terminally truncated Ror1 version, originating from one of the many transcript splice variants known for the *Ror1* gene (https://ics.hutton.ac.uk/eorna/index.html). A similar pattern to that observed in extracts from cv. Ingrid wild-type plants was also detected in extracts of BC Ingrid *mlo-5* mutant plants (Figure 3). By contrast, extracts of most *mlo-5 ror1* double mutants lacked both characteristic bands, except for the *mlo-5 ror1-1* and *mlo-5 ror1-2* double mutants, which had strong and faint Ror1 bands, respectively. The lack of detectable approximately 170 kDa bands in the case of the *mlo-5 ror1-3* to *mlo-5 ror1-7* double mutants is consistent with the type of mutational events detected in the *Ror1* gene in these mutants (Table 1), which are predicted to result in either the absence of Ror1 (*mlo-5 ror1-4*) or severely truncated versions thereof (*mlo-5 ror1-3, mlo-5 ror1-5, mlo-5 ror1-6*, and *mlo-5 ror1-7*). The latter might be unstable *in planta*, and, except for *ror1-7*, which has a frame-shift mutation in the C-terminal region, would be undetectable with the C-terminus-specific antiserum. The simultaneous absence of the approximately 110 kDa band in addition to

Table 1 Molecular characteristics of *ror1* mutants

Mutant allele	Mutant designation	Mutagen[a]	Effect at the level of genomic DNA[b]	Effect at the level of coding sequence[c]	Predicted effect at protein level[d]	Reference for the mutant
ror1-1	A39	EMS	$G^{17666} \to A$	$A^{2144} \to G$	$Gly^{715} \to Glu$ ($G^{715}E$)	Freialdenhoven et al. (1996)
ror1-2	A89	EMS	$A^{3328} \to G$	$G^{467} \to A$	$Gly^{156} \to Glu$ ($G^{156}E$)	Freialdenhoven et al. (1996)
ror1-3	C36	NaN$_3$	$G^{23136} \to A$	$\Delta^{3202-3218}$	Frame shift after S^{1067}, resulting in a premature stop codon	Freialdenhoven et al. (1996)
ror1-4	C69	NaN$_3$	Unknown	mRNA undetectable	Protein absent	Freialdenhoven et al. (1996)
ror1-5	C88	NaN$_3$	$G^{23136} \to A$	$\Delta^{3202-3218}$	Frame shift after S^{1067}, resulting in a premature stop codon	Freialdenhoven et al. (1996)
ror1-6	C33	NaN$_3$	$G^{7858} \to A$	Insertion of 12 nucleotides (from intron) after G^{1494}	Frame shift after K^{498}, resulting in a premature stop codon	Acevedo-Garcia et al. (2013)
ror1-7	C82	NaN$_3$	$G^{29039} \to A$	Insertion of 31 nucleotides (from intron) after A^{4329}	Frame shift after E^{1443}, resulting in a premature stop codon	Acevedo-Garcia et al. (2013)

[a]EMS, ethyl methanesulfonate; NaN$_3$, sodium azide.
[b]Numbering according to the *HORVU.MOREX.r3.1HG0046420* genomic sequence (30 326 bp) from cv. Morex in EnsemblPlants (Release 52) – see also Data S1.
[c]Numbering according to the *HORVU.MOREX.r3.1HG0046420* coding sequence (4527 bp) from cv. Ingrid as derived in this study (Data S1).
[d]Numbering according to the HORVU.MOREX.r3.1HG0046420 amino acid sequence deduced from cv. Ingrid as derived in this study (Data S1).
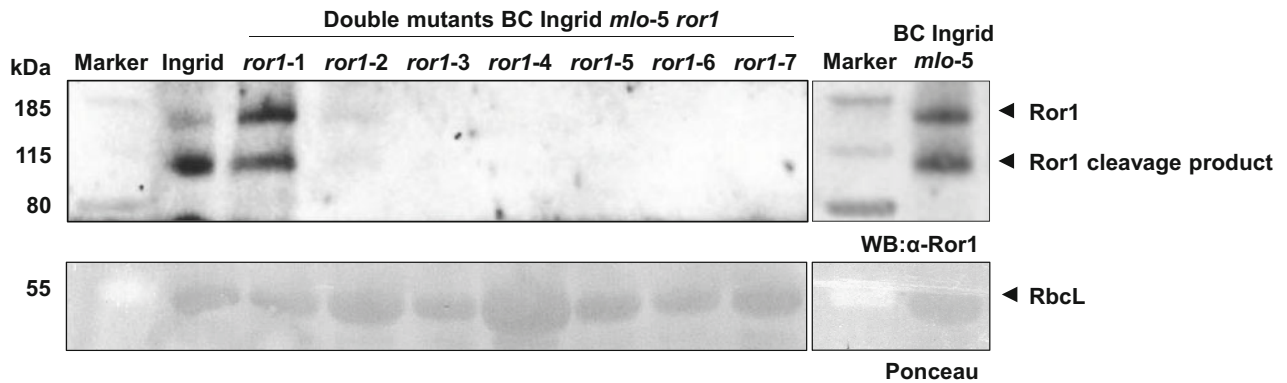
Figure 3. Immunoblot analysis of *mlo ror1* double mutants. Immunoblot showing Ror1 protein accumulation in leaves of wild-type (cv. Ingrid, *Mlo Ror1* genotype), various *mlo*-5 *ror1* double mutant, and BC Ingrid *mlo*-5 mutant plants. Total protein was extracted from leaves and separated by SDS-PAGE and blotted onto nitrocellulose membranes, which were probed with polyclonal α-Ror1 antiserum. Staining of the nitrocellulose membrane with Ponceau S, showing the prominent band of the ribulose-1,5-bisphosphate carboxylase/oxygenase (Rubisco) large subunit (RbcL), served as an indicator of protein loading and transfer. Molecular masses (in kDa) are given on the left according to the protein marker used. The experiment was repeated once with a similar outcome.

the approximately 170 kDa signal in a subset of the *mlo*-5 *ror1* double mutants further supports the notion that this band represents a cleavage product derived from Ror1. The polyclonal α-Ror1 antiserum thus appears to be specific for the Ror1 myosin and does not cross-react with other barley myosins.

The only stable Ror1 mutant variant, encoded by *ror1*-1 (Figure 3), is characterized by a glycine-to-glutamic acid substitution at amino acid position 715 ($G^{715}E$). This glycine residue is common to all myosins, except for some members of the Stramenopiles-specific class-32 and class-33 myosins, and is located at the very end of the motor domain, being part of the so-called converter region (Figure S5). According to the X-ray-resolved three-dimensional structure of the motor domain of the intracellular cargo-transporting chicken myosin Myo5A (Coureux et al., 2004), this glycine is located at the interface of the converter region and the relay-loop of the myosin motor domain (Figure 4a,b). The *ror1*-2 mutant, which shows a very weak Ror1 band in immunoblot analysis (Figure 3), indicating low accumulation of this variant, is also characterized by a glycine-to-glutamic acid substitution in the *Ror1* coding sequence. This replacement affects amino acid 156, which is another highly conserved amino acid in myosins (Figure S5) and is located at the N-terminal end of the phosphate-binding P-loop in the ATPase domain of the myosin motor head (Figure 4a,c).

Ror1 protein levels increase transiently during powdery mildew infection

RNA-Seq data obtained with different *ror1* mutants (Table S3) indicate increased *Ror1* transcript accumulation in the course of the barley–powdery mildew interaction, suggesting that *Ror1* expression is pathogen-responsive. Since transcript and protein levels do not necessarily correlate and protein levels are functionally more relevant than

transcript levels, we next focused on exploring the dynamics of Ror1 protein accumulation in the course of fungal pathogenesis. Using the specific α-Ror1 antiserum, we studied the accumulation of Ror1 myosin by immunoblot analysis in a time-course experiment following inoculation with *B. hordei* conidiospores in cv. Ingrid wild-type plants (*Mlo Ror1* genotype; compatible interaction). We noticed a transient increase in Ror1 levels during the course of infection, with the strongest band intensities seen between 24 and 72 hpi and a decrease thereafter. The approximately 110-kDa cleavage product followed a similar pattern (Figure 5). In two out of the three replicates of the experimental time courses, we observed a shift in relative signal intensities for the full-length Ror1 protein and its presumed cleavage product at later time points. While in protein extracts from pathogen-free (non-inoculated) samples (at 0 h) both Ror1 forms exhibited similar steady-state levels, in these two replicates the approximately 110-kDa fragment steadily increased in abundance relative to the approximately 170-kDa full-length protein over the course of infection, possibly as a consequence of enhanced host- and/or pathogen-associated protease activities during fungal pathogenesis (Figure 5). Taken together, these data indicate a pathogen-triggered transient accumulation of Ror1 myosin, consistent with its genetically defined role as a component of antifungal defense in barley.

Pharmacological inhibition experiments suggest that Ror1 is the only barley myosin involved in *mlo* resistance

Next, we wondered whether other myosins besides Ror1 could be involved in *mlo*-based resistance. Although genetic analysis (forward genetics) revealed mutations only in *Ror1* and *Ror2* (the latter encoding a t-SNARE protein; Collins et al., 2003; Freialdenhoven et al., 1996), it remains a formal possibility that additional barley myosin paralogs may contribute to antifungal defense in *mlo*
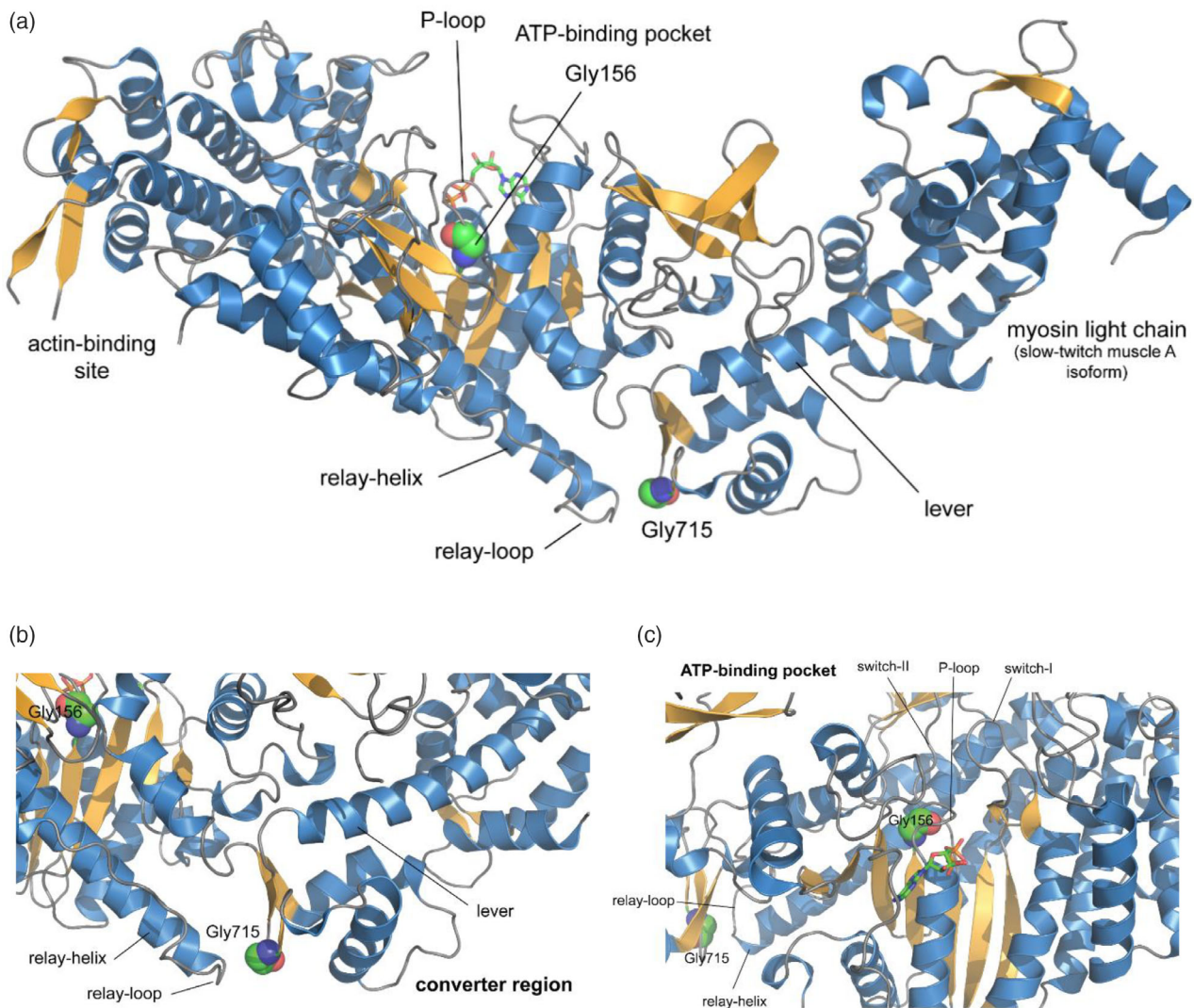
Figure 4. Predicted localization of single amino acid substitutions caused by the *ror1*-1 and *ror1*-2 mutations within the myosin motor domain. (a) Experimentally determined three-dimensional structure of the motor domain of chicken Myo5A (pdb-id 1W7I; Coureux et al., 2004) with bound ADP (drawn as sticks). The structure extends up to the first IQ motif and includes a myosin light chain molecule wrapping around the lever. The two glycine residues affected in the *ror1*-1 and *ror1*-2 mutants (Gly[156] and Gly[715]), which are invariant across nearly all myosins, are shown as spheres. (b) Close-up view into the converter region of the motor domain of chicken Myo5A. Gly[715] is an important part of the interface between the relay-loop and the converter domain. (c) Close-up view of the ATP-binding pocket of the motor domain of chicken Myo5A. The ADP molecule is drawn as sticks and the two glycine residues are shown as spheres. Gly[156] is located at the N-terminus of the P-loop. The glycine residues are numbered according to the *H. vulgare* Myo11A1 (Ror1) sequence for better orientation.

mutants. These might not become apparent in the form of mutant plants, e.g., due to functional redundancy or lethality upon loss of function. To investigate this option experimentally, we used the established myosin inhibitor NEM, which prevents ATP binding to myosin (Meeusen & Cande, 1979; Radford & White, 2011).

We first subjected leaves of the BC Ingrid *mlo*-5 mutant to various NEM concentrations (0.25, 0.5, and 5 mM), inoculated the inhibitor-treated leaves with *B. hordei* conidiospores of isolate K1, and assessed the success of fungal infection microscopically. Mock-treated BC Ingrid *mlo*-5 leaves had a median *B. hordei* entry rate of approximately 2%, which increased to approximately 10% for leaves treated with 0.25 mM NEM. Higher NEM concentrations resulted in a decrease in *B. hordei* host cell entry (approximately 6% for 0.5 mM NEM and approximately 1% for 5 mM NEM), possibly due to toxic effects on the host and/or the pathogen at higher concentrations. The values determined for the BC Ingrid *mlo*-5 mutant at 0.25 and 0.5 mM NEM correspond well to the *B. hordei* entry rate on leaves of the mock-treated *mlo*-5 *ror1*-4 double mutant (approximately 8%; Figure S6). In sum, these data suggest that NEM treatment can partially break *mlo* resistance, probably by impairing myosin function.
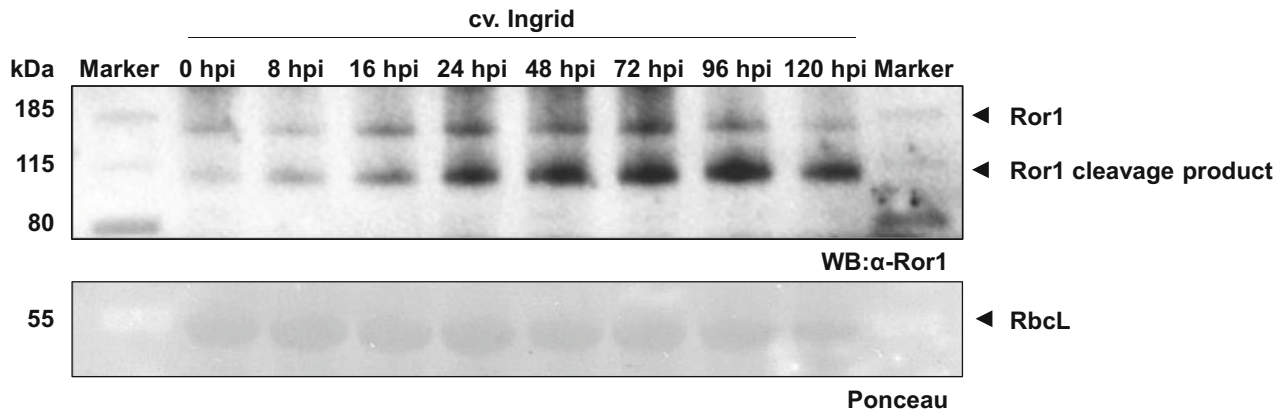
Figure 5. Ror1 protein levels increase transiently during powdery mildew pathogenesis. Immunoblot showing Ror1 protein accumulation in leaves of wild-type (cv. Ingrid, *Mlo Ror1* genotype) plants in the course of *B. hordei* (isolate K1) infection. Leaves were sampled at the indicated time points after inoculation, and total protein was extracted, separated by SDS-PAGE, and transferred onto nitrocellulose membranes, which were probed with polyclonal α-Ror1 antiserum. Staining of the nitrocellulose membrane with Ponceau S, showing the prominent band of the ribulose-1,5-bisphosphate carboxylase/oxygenase (Rubisco) large subunit (RbcL), served as an indicator of protein loading and transfer. Molecular masses (in kDa) are given on the left according to the protein marker used. In independent time-course immunoblot experiments covering different periods after *B. hordei* inoculation, similar pathogen-triggered Ror1 accumulation kinetics were observed.

We next extended the experiment by subjecting leaves of the BC Ingrid *mlo*-5 *ror1*-4 double mutant to NEM treatment before *B. hordei* conidiospore inoculation. Mock treatment of this genotype resulted in a *B. hordei* entry rate of approximately 8%, which increased only slightly upon exposure to 0.25 mM NEM (approximately 12%) and declined at higher NEM concentrations (approximately 6% for 0.5 mM NEM and approximately 5% for 5 mM NEM; Figure S6). Since we did not detect a significant increase of *B. hordei* host cell entry following NEM treatment, we conclude that Ror1 is probably the only barley myosin that contributes to *mlo* resistance.

ROR1 partially colocalizes with peroxisomes

We next aimed to study the subcellular localization of Ror1 by taking advantage of particle bombardment-based transient gene expression in single barley leaf epidermal cells (Panstruga, 2004). To this end, we generated plasmid constructs designed to express N- and C-terminally yellow fluorescent protein (YFP)-tagged variants of Ror1. To test whether they retain their functionality despite the presence of the attached fluorophore, we expressed these constructs and a control construct designed to express untagged Ror1 (all under the control of the constitutive maize [*Zea mays*] *ubiquitin* promoter) in an *mlo ror1* double mutant to explore their capacity to complement the mutant phenotype. Expression of *Mlo* served as a positive control in this experimental setup, and coexpression of β-glucuronidase (GUS; encoded by *uidA*) was used to identify successfully transformed cells (Panstruga, 2004). After particle bombardment, detached leaf specimens were inoculated with *B. hordei* conidiospores to assess the successful entry of powdery mildew into transformed, *uidA*-positive cells by scoring the presence or absence of fungal haustoria. Expression of the *uidA* marker gene alone (negative control) in the BC Ingrid *mlo*-5 *ror1*-5 double mutant resulted in a median *B. hordei* entry rate of approximately 16%, while *Mlo* overexpression (together with the *uidA* reporter) resulted as expected in approximately 85% host cells accommodating *B. hordei* haustoria in this genotype (positive control). Coexpression of the candidate *Ror1* gene *HORVU.MOREX.r3.1HG0046420* with *uidA* resulted in approximately 5% *B. hordei* entry (i.e., a significant reduction as compared to the *uidA* only negative control), indicating complementation of the *ror1* phenotype by restoring near-complete resistance to the powdery mildew pathogen (Figure 6a). This result corroborates that *HORVU.MOREX.r3.1HG0046420* is *Ror1*. Additionally, similar to unlabeled Ror1, both fluorophore-labeled Ror1 versions markedly enhanced resistance in the BC Ingrid *mlo*-5 *ror1*-5 background when coexpressed with the *uidA* reporter (Figure 6a), suggesting that these Ror1 variants are functional.

We then analyzed the subcellular localization of the fluorophore-tagged Ror1 fusion proteins by confocal laser scanning microscopy of bombarded cells. We found that the YFP-labeled Ror1 variants exhibit nucleo-cytoplasmic localization. The fluorescence signal was partly associated with mobile punctate structures that were reminiscent of peroxisomes in terms of number and size (Figure 6b). To investigate a putative colocalization of Ror1 with peroxisomes, we coexpressed the YFP-tagged Ror1 variants with a fluorescent peroxisomal marker protein (DsRed-PTS1). Superimposition of the YFP and DsRed fluorescent signals showed partial colocalization, regardless of the position of the Ror1-YFP label (N- or C-terminal; Figure 6b). As
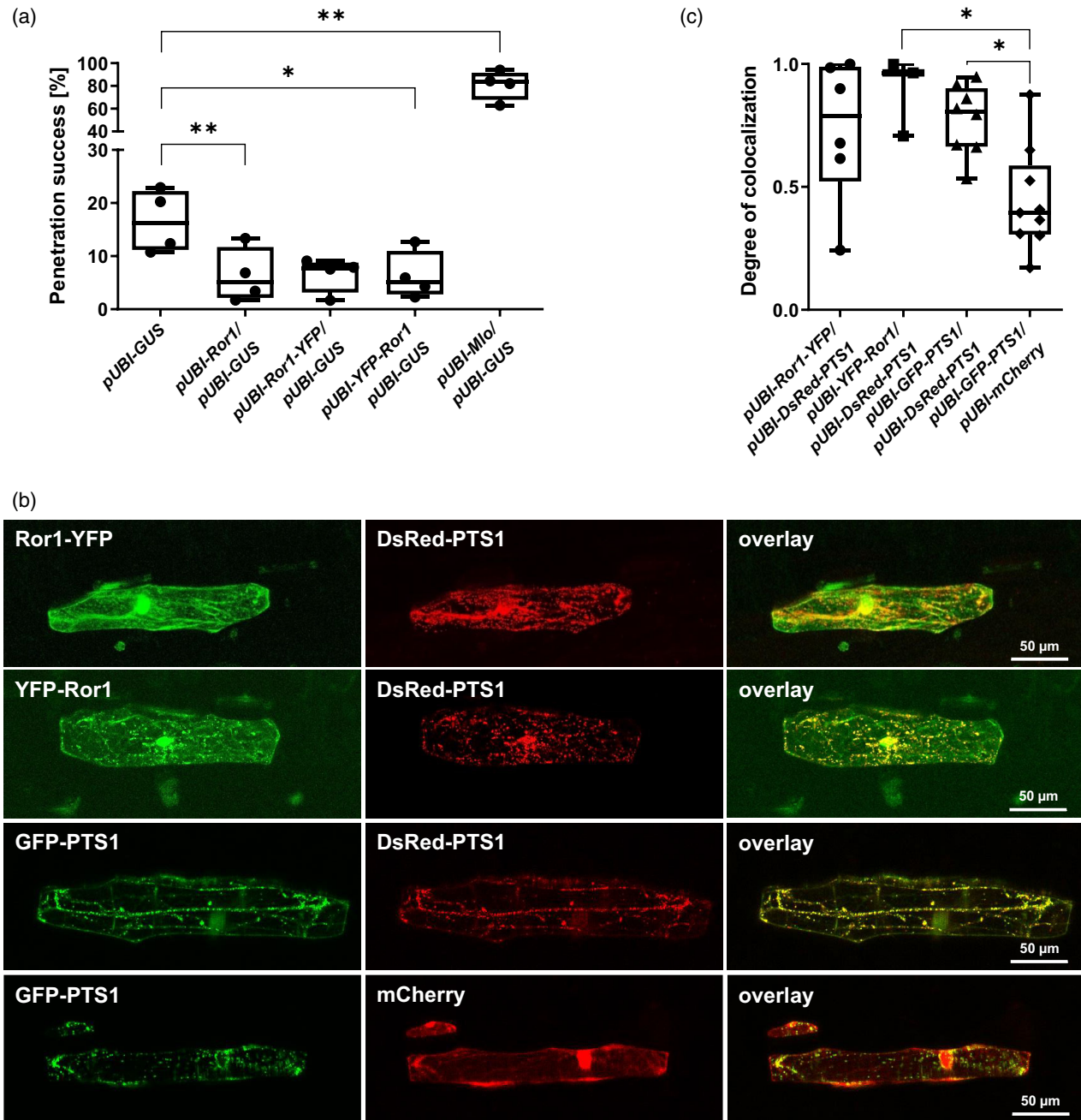
Figure 6. Endomembrane compartments labeled by fluorophore-tagged Ror1 partially colocalize with peroxisomes. (a) The fluorophore-tagged Ror1 variants are functional. Detached barley leaves (genotype *mlo*-5 *ror1*-5) were (co-)bombarded with the indicated constructs and specimens inoculated with *B. hordei* isolate K1 at 4 h after the bombardment. Leaves were subjected to staining for GUS activity at 48 hpi. Host cell entry rates were scored microscopically and are given as the percentage of germinated *B. hordei* sporelings that succeeded in haustorium formation. Data shown are based on four biological replicates with a minimum of 50 (typically 100–200) analyzed cells per replicate and construct combination, yielding in total at least 450 analyzed cells per construct combination. Statistical analysis was performed using one-way ANOVA on paired datasets with the Geisser–Greenhouse correction and a Dunnett *post hoc* test to correct for multiple comparisons. Asterisks indicate statistically significant differences from the pUBI-GUS control (*$P < 0.05$, **$P < 0.01$). (b) Representative micrographs of YFP-tagged Ror1 subcellular localization. The following plasmids were co-delivered *via* particle bombardment in detached leaves of the barley *mlo*-5 *ror1*-5 double mutant: pUBI-Ror1-YFP in combination with pUBI-DsRed-PTS1, pUBI-YFP-Ror1 in combination with pUBI-GFP-PTS1 in combination with pUBI-DsRed-PTS1, and pUBI-GFP-PTS1 in combination with pUBI-mCherry. At 24–48 h after bombardment, specimens were observed by confocal laser scanning microscopy. The overlay panels illustrate superimposed YFP/GFP and DsRed/mCherry signals. Micrographs represent maximum projections of Z-stacks. (c) Quantification of colocalization of YFP/GFP and DsRed signals in co-bombarded barley cells. Colocalization was assessed with CellProfiler software as described in the Experimental Procedures section and is based on six (pUBI-Ror1-YFP/pUBI-DsRed-PTS1), three (pUBI-YFP-Ror1/pUBI-DsRed-PTS1), eight (pUBI-GFP-PTS1/pUBI-DsRed-PTS1), or nine (pUBI-GFP-PTS1/pUBI-DsRed) analyzed cells. Statistical analysis was performed using one-way ANOVA with a Tukey *post hoc* test to correct for multiple comparisons. Asterisks indicate statistically significant differences (*$P < 0.05$) between samples.

positive and negative controls we coexpressed peroxisome-localized GFP and DsRed marker proteins (GFP-PTS1 and DsRed-PTS1) and peroxisome-localized GFP in combination with cytosolic mCherry, respectively (Figure 6b). We quantified the degree of colocalization of the YFP and DsRed fluorescent signals and found a median overlap of >75%, similar to the GFP-PTS1/DsRed-PTS1 positive control, while the degree of colocalization for the GFP-PTS1/mCherry combination was markedly lower (median overlap <50%). Together, these results indicate a clear yet incomplete association of the Ror1 myosin with peroxisomes (Figure 6c).

Expression of the Ror1 tail domain exerts a dominant-negative effect and phenocopies a *ror1* mutant

Expression of the C-terminal tail domain of myosins is known to cause a dominant-negative effect on the function of different myosin classes in various experimental systems, including plants (Avisar et al., 2009; Bittins et al., 2009; Burns et al., 1995; Stephan et al., 2021). We, therefore, wondered whether (over)expression of the Ror1 tail domain would also lead to a dominant-negative effect. We took advantage of the above described biolistic transient gene expression in single leaf epidermal cells in combination with a *B. hordei* challenge and expressed the tail region of *Ror1* (corresponding to amino acids 879–1509) under the control of the constitutive maize *ubiquitin* promoter in leaf epidermal cells of BC Ingrid *mlo*-5 mutant plants. Biolistic delivery of the *uidA* reporter construct alone resulted in approximately 4% median *B. hordei* host cell entry, consistent with the high resistance level of this genotype. By contrast, coexpression of *uidA* with the positive control *Mlo* resulted in complementation of the *mlo* resistant phenotype and restoration of susceptibility to the powdery mildew pathogen (approximately 71% *B. hordei* entry rate). Transient coexpression of the *uidA* reporter with the *Ror1* tail region resulted in an intermediate outcome (approximately 24% *B. hordei* entry; Figure 7). This level of fungal ingress corresponds well to the entry rates known from *mlo*-5 *ror1* double mutant plants (Freialdenhoven et al., 1996) and also agrees with the outcome of the transient expression of the *uidA* reporter in the background of the *mlo*-5 *ror1*-5 double mutant (approximately 16%; cf. Figure 6a). Thus, we conclude that (over)expression of the *Ror1* tail domain in the *mlo* background phenocopies an *mlo ror1* double mutant, which is indicative of a dominant-negative effect mediated by this construct. To test the specificity of this effect, we examined the tail regions of two additional barley myosins, HORVU6Hr1G091010 (Myo11A3; amino acids 878–1511) and HORVU6Hr1G081340 (Myo11G1; amino acids 876–1497), in the biolistic gene expression assay. Transient coexpression of these tail constructs with the *uidA* reporter failed to increase *B. hordei* entry levels beyond the range of *uidA*
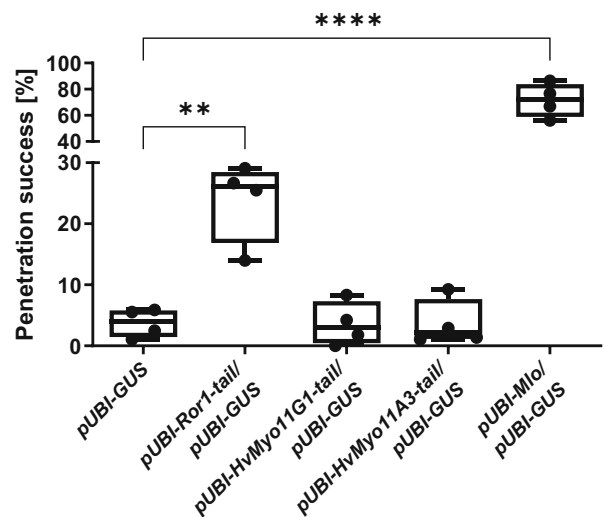

Figure 7. Transient overexpression of the Ror1 tail fragment exerts a dominant-negative effect. Detached barley leaves (genotype BC Ingrid *mlo*-5) were (co-)bombarded with the indicated constructs and specimens inoculated with *B. hordei* isolate K1 at 4 h after the bombardment. Leaves were subjected to staining for GUS activity at 48 hpi. Host cell entry rates were scored microscopically and are given as the percentage of germinated *B. hordei* sporelings that succeeded in haustorium formation. Data shown are based on four biological replicates with a minimum of 50 (typically 100–200) analyzed cells per replicate and construct combination, yielding in total at least 300 analyzed cells per construct combination. Statistical analysis was performed using one-way ANOVA with a Dunnett *post hoc* test to correct for multiple comparisons. Asterisks indicate statistically significant differences from the pUBI-GUS control (**$P < 0.01$, ****$P < 0.0001$).

negative control in the *mlo* mutant background (Figure 7), indicating the specificity of the dominant-negative effect of the *Ror1* tail.

DISCUSSION

We report the identification of barley *Ror1* (*HORVU.MOREX.r3.1HG0046420*) as a gene encoding the class XI myosin isoform HvMyo11A (Figure 2). Its genomic position was ultimately narrowed down by a combination of synteny-guided map-based cloning (Acevedo-Garcia et al., 2013; Collins et al., 2001), the Hi-C barley genome assembly (Mascher et al., 2017), and RNA-Seq analysis of a collection of *ror1* mutants (this study). Suppression of meiotic recombination in the pericentromeric region and breaks in barley–rice synteny made it difficult to isolate the gene in previous attempts. In retrospect, the *Ror1* target interval was found to be approximately 10 Mb in size, as calculated from the recently released long read-based updated barley genome assembly (Mascher et al., 2021), showing the formerly deduced gene order (Table 2). According to this latest genome assembly, the previously identified *Ror1*-flanking markers, *Con* and *Pol* (Acevedo-Garcia et al., 2013), are approximately 8.3 Mb apart. Given that, based on 2798 meioses tested, only 1 and 4 meiotic

Table 2 Gene order at the *Ror1* locus

Gene designation[a]	GenBank accession number	Morex genome assembly v3 gene identifier[b]	Position on barley chromosome 1H [bp][b]
Myo	AK370653	*HORVU.MOREX.r3.1HG0045720*	298981770...298991834
Ltp	AK372510	*HORVU.MOREX.r3.1HG0045730*	298992113...298993044
Ppr	XM_045102778	*HORVU.MOREX.r3.1HG0045750*	299141478...299143564
Pol	AK375542	*HORVU.MOREX.r3.1HG0045780*	299472431...299487080
Mat	AK250432	*HORVU.MOREX.r3.1HG0045830*	299939164...299943309
Noc	XM_045093166	*HORVU.MOREX.r3.1HG0045870*	300319076...300323749
α-Galactosidase	AK250464	*HORVU.MOREX.r3.1HG0046150*	303581212...303586895
Ror1	XM_045115395	*HORVU.MOREX.r3.1HG0046420*	305898717...305927840
Con	AK371545, AK355699	*HORVU.MOREX.r3.1HG0046850*	307791235...307794751
Unk	AK363338	*HORVU.MOREX.r3.1HG0046920*	308151884...308160421
Dep	AK353904	*HORVU.MOREX.r3.1HG0047060*	308667145...308669156
Oxp	AK354544	*HORVU.MOREX.r3.1HG0047080*	308681414...308685617

[a]According to (Acevedo-Garcia et al., 2013), except for *α-galactosidase*, which was only mentioned by its GenBank accession number.
[b]According to (Mascher et al., 2021).

recombination events were found between *Ror1* and *Con* and between *Ror1* and *Pol*, respectively, resulting in genetic distances of 0.036 cM and 0.143 cM for these intervals (Acevedo-Garcia et al., 2013), the ratio of physical to genetic distance is approximately 46 Mb/cM in the *Ror1* target region. This value is more than 10 times higher than the reported average ratio of 3.7–4.2 Mb/cM for the barley genome as a whole (DeScenzo & Wise, 1996), which exhibits an average of 1.5 Mb/cM in the distal portions of chromosome arms and up to 89 Mb/cM near the centromeres (Stephens et al., 2004).

Myosins are motor proteins that enable intracellular transport processes along actin cytoskeleton tracks. *HORVU.MOREX.r3.1HG0046420* (*Ror1*) is one out of 12 barley myosin genes, of which two encode class VIII and 10 encode class XI myosins (Figure S1; Figure 2). Class VIII and class XI myosins differ by the length of their lever arms and their coiled-coil domains (Tominaga & Nakano, 2012). While class VIII myosins have been associated with cytokinesis (Reichelt et al., 1999; Wu & Bezanilla, 2014) and plasmodesmal functions (Avisar et al., 2008), class XI myosins have been primarily implicated in vesicle trafficking and organelle transport (Li & Nebenführ, 2007; Peremyslov et al., 2008; Peremyslov et al., 2012). Like most plant myosins, *Ror1* is dispensable for barley growth and reproduction in laboratory or greenhouse environments, as indicated by the full viability and lack of obvious pleiotropic phenotypes in the *ror1*-4 null mutant. The closest homologs in *A. thaliana* and thus presumptive orthologs of *HvMyo11A1* according to the motor domain phylogeny are *AtMyo11A1* (*XI-A*; *At1g04600*) and *AtMyo11A2* (*XI-D*; *At2g33240*) (Figure 2). Surprisingly, these two *A. thaliana* genes are primarily expressed in pollen (Peremyslov et al., 2011; Sparkes, 2011), with negligible expression levels in rosette leaves and no evidence of biotic stress-induced increase in transcript accumulation

(http://bar.utoronto.ca/). Consistent with a putative role in sexual reproduction for these two myosins, reduced seed set has been observed in *AtMyo11A1* mutant plants (Madison et al., 2015). No other mutant phenotype has been reported for these two genes so far. The distinctive expression pattern of *HORVU.MOREX.r3.1HG0046420*, which is expressed ubiquitously at medium levels in barley tissues (https://www.ebi.ac.uk/gxa/home), suggests that plant lineage- or species-specific diversification of regulatory sequences has driven or contributed to a functional diversification of myosin orthologs in different biological processes in flowering plants. Using the motor domain-based myosin phylogeny, the functionally yet uncharacterized rice protein encoded by gene *Os02g0545000* is the presumptive ortholog of Ror1 (Figure 2). The non-syntenic location of this gene on rice chromosome 2 (rather than rice chromosome 10) explains why we have not been able to localize barley *Ror1 via* a synteny-based approach (Acevedo-Garcia et al., 2013; Collins et al., 2001). Given that the flanking genes of *Ror1* within the Hi-C-ordered BAC clusters are largely collinear to the syntenic region on rice chromosome 10 (Table S1), the non-syntenic position of *Os02g0545000* presumably results from the translocation of a single gene or a small genomic region to rice chromosome 2 (or, alternatively, the insertion of such a segment on barley chromosome 1). Manual inspection of the genes neighboring *Os02g0545000* on rice chromosome 2 indeed revealed no evidence for additional instances of interchromosomal gene translocation.

Plant cells attacked by filamentous pathogens undergo dynamic changes and extensive reorganization and polarization toward the site of attempted ingress (Lipka & Panstruga, 2005; Park et al., 2018; Schmelzer, 2002). This involves confined cytoplasmic aggregation (Takemoto et al., 2003), relocation of organelles such as mitochondria and peroxisomes (Fuchs et al., 2016; Hématy et al., 2020),

polarized reorganization of cytoskeletal elements (actin filaments and microtubules) (Opalski et al., 2005), the formation of localized cell wall reinforcements (papillae) (Malinovsky et al., 2014), and redistribution of a subset of plasma membrane-resident proteins (Bhat et al., 2005). In particular, cytoskeletal reorganization has been found to be critical for effective pre-invasive resistance to filamentous pathogens. Pharmacological (Kobayashi & Hakuno, 2003; Moral et al., 2017) or genetic interference (Miklis et al., 2007) in actin filament integrity interferes with actin dynamics and permits enhanced invasion of fungal intruders. It is conceivable that motor protein-dependent transport processes contribute to this pathogen-inducible cellular restructuring, and here we identified a single class XI myosin as a critical component for extracellular resistance. The potential cargo of such intracellular transport activities might comprise vesicles, organelles, and other macromolecular complexes. Vesicle transport may be linked to the targeted delivery of proteins, antimicrobials, or cell wall components. On the other hand, the polar congregation of organelles underneath pathogen contact sites could serve to shorten transport pathways for intracellular communication (e.g., in the case of the nucleus) and/or enable metabolic channeling for cellular activities such as the biosynthesis of defense-related molecules.

In *A. thaliana*, combined genetic and biochemical analyses unraveled two separate pathways contributing to pre-invasive immunity against powdery mildews and other tested filamentous pathogens. One pathway involves the t-SNARE protein PEN1 and likely the formation of ternary SNARE complexes with its partner SNARE proteins SNAP-34 and VAMP721/VAMP722, resulting in presumed vesicle fusion events at the host plasma membrane beneath incipient pathogen invasion sites (Kwon et al., 2008). The cargoes of this vesicular transport route have remained elusive. The second pathway comprises the myrosinase PEN2 (Lipka et al., 2005), the plasma membrane-resident ABC transporter PEN3 (Bednarek et al., 2009), and the phytochelatin synthase PEN4 (Hématy et al., 2020). PEN2 has been shown to hydrolyze indole glucosinolates, a class of sulfur-containing secondary metabolites, to form products that could act as broad-spectrum toxins and confer antifungal defense in the extracellular space (Bednarek et al., 2009). PEN4 relocates upon pathogen attack and is subsequently colocalized on immobilized mitochondria together with PEN2 underneath pathogen contact sites (Fuchs et al., 2016; Hématy et al., 2020). PEN4 acts in the PEN2 metabolic pathway, the products of which are presumably delivered to the extracellular space *via* the PEN3 ABC transporter. The previously described barley Ror2 t-SNARE is the ortholog and thus likely the functional equivalent of *A. thaliana* PEN1. Ror2 is probably also active in vesicle fusion at the plasma membrane as gene silencing

of barley *SNAP34* specifically impairs *mlo* resistance, and this encoded adapter SNARE protein interacts with the Ror2 t-SNARE in yeast two-hybrid assays (Collins et al., 2003) and together with Ror2 and the barley VAMP721 v-SNARE can form ternary SNARE complexes *in planta* (Kwaaitaal et al., 2010). The identification of Ror1 as a myosin motor protein reported here may at first glance extend this scenario by adding a potential vesicle carrier to the pathway. However, previous genetic data suggest that, similar to *A. thaliana*, two separate pathways, represented by Ror1 and Ror2, contribute to extracellular immunity against powdery mildew in barley. This notion is based on the finding that *mlo*-5 *ror1*-4 *ror2*-1 triple mutant plants show an additive effect on *B. hordei* host cell entry and fungal mycelium density on the leaf surface compared to the corresponding *mlo*-5 *ror1*-2 and *mlo*-5 *ror2*-1 double mutants (Collins et al., 2003). The fact that our work has now identified the *ror1*-4 mutant as a null mutant (Table 1) underlines the idea that Ror1 and Ror2 act in two genetically distinct pathways.

The myosin motor Ror1 is not exclusively involved in *mlo*-dependent extracellular disease resistance, as *Mlo ror1-2 Ror2* (i.e., *ror1*-2 single mutant) plants are hypersusceptible to *B. hordei* entry compared to *Mlo Ror1 Ror2* wild-type siblings (Collins et al., 2003), suggesting that Mlo negatively regulates Ror1 activity in pre-invasive immunity during compatible interactions. Barley Mlo engages in a Ca^{2+}-dependent interaction with calmodulin *in vitro*, and loss of calmodulin binding in the cytoplasmic C-terminal tail of Mlo halves the ability to regulate defense against powdery mildew (Kim et al., 2002). The identification of the myosin motor Ror1 in this study, which contains six calmodulin-binding IQ motifs (Figure 2b), is consistent with the idea that the activities of the corresponding antagonistically acting Mlo and Ror1 proteins are coordinately modulated by pathogen-induced cytoplasmic Ca^{2+} transients and calmodulin.

In *A. thaliana*, genetic analysis has already shown that myosins play a role in pre-invasion resistance to adapted and non-adapted powdery mildew pathogens. Four phylogenetically distinct but highly expressed *A. thaliana* class XI myosins (*At*Myo11F, *At*Myo11B2, *At*Myo11G, and *At*Myo11E) have been found to cofunction in the dynamic cellular reorganization of actin filaments and redistribution of organelles upon pathogen attack, contributing to limit host cell entry beneath pathogen contact sites (Yang et al., 2014). The enhanced susceptibility phenotype of the respective myosin quadruple mutant was particularly striking for the non-adapted barley powdery mildew pathogen, i.e., in the context of non-host resistance, which shares several common features with *mlo*-based penetration resistance (Humphry et al., 2006). Surprisingly, none of these four myosins identified by the study of Yang and coworkers (Yang et al., 2014) is phylogenetically closely

related to Ror1 (*Hv*Myo11A1; Figure 2). These findings hint at a differential contribution of myosin isoforms in the dicotyledonous plant *A. thaliana* and monocotyledonous barley in pre-invasive defense to powdery mildews. This situation differs from the conserved contribution of orthologous t-SNARE proteins (PEN1 in *A. thaliana* and Ror2 in barley) to *mlo*-mediated resistance (Collins et al., 2003; Consonni et al., 2006).

Class XI myosins are known to form homodimers and to walk processively along actin filaments in 35-nm steps (Tominaga et al., 2003). Based on immunolocalization experiments and the expression of fluorophore-labeled full-length and/or truncated versions, they have been localized to various organelles and are thought to drive actin-dependent organelle movement by direct association with these organelles. For example, in the case of *A. thaliana*, there is experimental evidence for the transport of peroxisomes by *At*Myo11B2, of nuclei by *At*Myo11G myosins, and of the endoplasmic reticulum and vesicles by *At*Myo11E myosins (reviewed in Madison & Nebenführ, 2013). We found that functional YFP-tagged Ror1 expressed in barley leaf epidermal cells is nucleo-cytoplasmically distributed and partially localizes to mobile punctate cellular structures that partially overlap with fluorophore-marked peroxisomes (Figure 6). Thus, we conclude that the Ror1 myosin drives intracellular movement of multiple small endomembrane compartments, including peroxisomes, which might be crucial for antifungal defense at the cell periphery. Notably, a similar subcellular localization pattern was found for the YFP-tagged DIL domain of Ror1 (at the time termed Hv XI-2; Sattarzadeh et al., 2011), suggesting that the DIL domain might be the primary cargo-binding domain of Ror1. Further studies will be required to unveil the identity of the non-peroxisomal endomembrane compartments shuttled by Ror1 in leaf epidermal cells.

The partial nuclear localization of YFP-tagged Ror1 fusion proteins (Figure 6) might be surprising at first glance. However, various myosin isoforms localized in the nucleus have been reported in animal/human systems (de Lanerolle, 2012). Together with nuclear actin, nuclear myosins are thought to play various roles in regulating chromatin architecture and thus gene expression (Fili et al., 2017; Venit et al., 2020). Although the fluorescent nuclear signal could in principle originate from the *in planta* cleavage of the YFP tag from the Ror1 fusion proteins upon transient (over)expression, we consider this scenario less likely, as nuclear localization was observed independently of the position of the YFP fluorophore (N- or C-terminal; Figure 6). We, therefore, cannot exclude a role for Ror1 in the plant nucleus in the context of *mlo*-mediated resistance. To our knowledge, plant myosins have so far only been detected in association with the nuclear envelope, but not inside the nucleus (Tamura et al., 2013).

Only one of the seven characterized *ror1* mutant alleles encodes a protein variant whose accumulation level is similar to wild-type Ror1 (Figure 3). The respective mutational event causes an amino acid substitution ($G^{715}E$) that is thought to affect the relay–converter interface of the Ror1 myosin (Figure 4a,b). The relay helix is an essential element of the force-generating region of myosins, connecting the nucleotide-binding site and the converter domain. The converter domain, in turn, transmits and amplifies small conformational changes in the nucleotide-binding site to the lever arm, enabling the actual power stroke. It is known that the interface between the relay helix and the converter domain is critical for optimal myosin performance by fine-tuning myosin kinetics, in particular ATP binding and hydrolysis, as demonstrated by site-directed mutagenesis of *Drosophila melanogaster* skeletal muscle myosin II (Bloemink et al., 2016; Kronert et al., 2014; Ramanath et al., 2011). Currently, we do not know how exactly the $G^{715}E$ mutation affects Ror1 activity. Based on evidence from other cellular myosin systems, we speculate that the corresponding Ror1 variant has altered kinetic properties that prevent its proper function in antifungal defense, e.g., in the timely delivery of antimicrobial cargo, cell wall precursors, and/or organelles at the cell periphery beneath pathogen contact sites (see above).

The Ror1 myosin motor described in this work not only provides a starting point for identifying the cargoes needed for extracellular immunity in barley. In transgenic barley plants expressing functional fluorescent Ror1 fusion proteins under the control of native regulatory sequences in the *ror1* background, it should also be possible to determine the kinetics of intracellular transport processes in real time. Finally, reciprocal complementation of barley *ror1* single and *A. thaliana myo11F myo11B2 myo11G myo11E* quadruple mutants with the corresponding wild-type genes offers the possibility to critically test the functional equivalence of these myosin isoforms in grasses and eudicots.

EXPERIMENTAL PROCEDURES

Plant and fungal material

Seven chemically induced barley *mlo*-5 *ror1* double mutants (*mlo*-5 *ror1*-1 to *mlo*-5- *ror1*-7), the respective parental back-crossed *mlo*-5 mutant in the genetic background of cv. Ingrid (BC Ingrid *mlo*-5), the mutant *mlo*-3 in the background of cv. Malteria Heda, and the panel of barley recombinants within the *Ror1* genetic interval have been described before (Acevedo-Garcia et al., 2013; Freialdenhoven et al., 1996). Barley cv. Ingrid was used as a wild-type genotype (*Mlo Ror1*) in this study. As a virulent powdery mildew pathogen, *B. hordei* isolate K1 was employed for pathogen infection assays.

RNA extraction

Sample preparation for RNA-Seq was performed using the RNeasy Plant Mini Kit 74904 (Qiagen, Hilden, Germany) according to the guidelines of the manufacturer. RNA extraction of *ror1* mutant leaves for further confirmation by Sanger sequencing was performed using the Quick-RNA Plant Miniprep Kit from Zymo Research (Irvine, CA, USA). cDNA synthesis was carried out using the High-Capacity cDNA Reverse Transcription kit from Applied Biosystems™ (Darmstadt, Germany).

RNA-Seq analysis

RNA-Seq libraries were prepared from an input of 4 μg total RNA with a TruSeq RNA sample preparation kit (Illumina) according to the recommendations of the supplier (TruSeq RNA sample preparation v2 guide, Illumina). Libraries were quantified by fluorometry, immobilized, and processed onto a flow cell with a cBot (Illumina, San Diego, CA, USA) followed by sequencing-by-synthesis in paired-end mode with TruSeq v3 chemistry on a HiSeq2000 platform by the Max Planck-Genome-Centre Cologne, Germany (https://mpgc.mpipz.mpg.de/home/).

Bioinformatics analysis

For the mapping of RNA-Seq reads to Hi-C and BAC barley genomic sequences (Mascher et al., 2017), the program TopHat (Trapnell et al., 2009) was used to identify and map reads with splice junctions. TopHat makes use of the tool Bowtie (Langmead et al., 2009), which computes the actual alignment of the mapped read. Here, the left and right reads were mapped independently, otherwise default settings were used.

To detect mutations in the genetic target interval, RNA sequences from all seven RNA-Seq samples (six *mlo-5 ror1* mutants and BC Ingrid *mlo*-5) were aligned to the barley reference genome (MorexV3_pseudomolecules_assembly, assembly: GCA_904849725.1; https://www.ebi.ac.uk/ena/browser/view/GCA_904849725.1; Mascher et al., 2021) using bowtie2 (v. 2.3.5.1-gcc8; Langmead & Salzberg, 2012). Bam files were produced, sorted, and indexed using samtools (v. 1.10-gcc8) (Li et al., 2009). Then, variant calling for each of the samples was performed using bcftools (v. 1.10.2-gcc8). All vcf files were processed using the bcftools filter, which allowed the selection of variants only included in the target region (1H: 303581211–307794751). Further filtering was performed to remove natural variants (cultivar-specific differences between cv. Morex and cv. Ingrid) using the isec -n, and -complement options with bcftools. The variants were additionally filtered based on features such as homozygosity, mapping quality (MQ > 20), and coverage (DP > 10 reads). The resulting vcf files were then merged using Python 3.10.4 and only mutations G → A, A → G, G → INDEL, A → INDEL, C → T, and T → C were considered. Finally, visualization of variants was performed on IGV (igv/2.8.0-gcc8) (Thorvaldsdóttir et al., 2013) for manual validation of candidate mutational events.

Myosin sequence reconstruction and phylogenetic analysis

Myosin protein sequences for *A. thaliana* (At) and *O. sativa* ssp. *japonica* (Os_a) were obtained from CyMoBase (https://www.cymobase.org/cymobase; Odronitz & Kollmar, 2007). Myosin homologs for *H. vulgare* and *Hordeum pubiflorum* were reconstructed as described elsewhere (Kollmar & Mühlhausen, 2017). Maximum-likelihood topologies were generated with IQ-Tree v. 1.6.1 (Nguyen et al., 2015) using the JTTDCMut+I + G4 model

determined to be the best-fitting model according to the Bayesian Information Criterion by ModelFinder (Kalyaanamoorthy et al., 2017).

Generation of polyclonal α-Ror1 antiserum

For the generation of Ror1-specific polyclonal antibodies, the proximal part of the C-terminal Ror1 tail domain (corresponding to amino acids 917–1086) was amplified by PCR and cloned *via* the restriction sites *Bam*HI and *Hin*dIII into pRSET A (Thermo Fisher Scientific, Darmstadt, Germany). The used primers are listed in Table S4. For the production of a highly pure recombinant Ror1 protein fragment, competent *E. coli* Rosetta(DE3) cells were grown at 37°C to an OD_{600} of 0.8, and expression of the N-terminally glutathione *S*-transferase (GST)-tagged $Ror1^{917-1086}$ protein was induced by adding 1 mM isopropyl ß-D-1-thiogalactopyranoside. After overnight expression, $GST-Ror1^{917-1086}$ was immobilized by using 1 ml GSTrap affinity columns (GE Healthcare, Solingen, Germany) and the $Ror1^{917-1086}$ fragment was eluted by adding a GST-tagged PreScission protease at 4°C under constant agitation for 18 h. Successful cleavage and purity of the protein were confirmed by SDS-PAGE followed by Coomassie staining. The enriched $Ror1^{917-1086}$ (0.9 mg ml^{-1}) protein fragment was provided to Davids Biotechnology (Regensburg, Germany) for raising polyclonal antisera in rabbits followed by affinity purification of the produced antibodies according to in-house protocols of the company.

Protein extraction and immunoblot analysis

For protein accumulation experiments, the middle part of one barley leaf (approximately 2 cm) was homogenized and phenolic total protein extraction was performed as described before (Thomas et al., 2015). Isolated protein pellets were solubilized in 7 M urea/2 M thiourea and the protein concentration was determined using the Bradford protein assay (Bradford, 1976). Unless otherwise stated, 10 μg of total protein was used for the separation of proteins by SDS-PAGE. Protein samples were denatured in 1x NuPAGE LDS Sample buffer (Thermo Fisher Scientific) by boiling at 95°C for 5 min before gel loading. Thereafter, samples were subjected to SDS-PAGE (using 10% Bis-Tris protein gels and 3-(*N*-morpholino) propanesulfonic acid running buffer). After separation, proteins were transferred to a nitrocellulose membrane (0.2 μm, Carl Roth, Karlsruhe, Germany) in transfer buffer (250 mM Tris, 2 M glycine, 0.5% [w/v] SDS) followed by immunodetection. Primary polyclonal α-Ror1 antibodies were produced by Davis Biotechnologie (Regensburg, Germany) as described above. Secondary antibodies were purchased from Cell Signaling (7074, HRP-linked α-rabbit IgG, Frankfurt, Germany). Chemiluminescence detection of antigen–antibody complexes was performed with SuperSignal™ West Femto Western substrate (Thermo Fisher Scientific). As a loading control, nitrocellulose membranes were stained in Ponceau S (AppliChem GmbH, Darmstadt, Germany) solution and each experiment was repeated at least once with similar results.

Cloning of constructs for transient gene expression

The *Ror1* cDNA was originally synthesized by Life Technologies GmbH (Darmstadt, Germany) based on the predicted sequence information of barley cv. Ingrid and placed in pDONR221. Subsequent analysis revealed that an additional short exon at the very 5′ end comprising three additional amino acids is present and, thus, these amino acids were absent in the synthesized clone. A corrected cDNA was generated by PCR, including coding information for the three missing amino acids in the respective forward primer, and the approximately 1.26-kb *Pst*I/*Bam*HI N-terminal *Ror1*

fragment in pDONR221-*Ror1* was replaced. The corrected and sequence-validated full-size *Ror1* cDNA was used in all assays. For cloning of constructs in the respective pUBI-GWY-nos, pUBI-YFP-GWY-nos, or pUBI-GWY-YFP-nos destination vectors by Gateway® technology, the following sequences were used: *Ror1* (*Hv*Myo11A1, *HORVU.MOREX.r3.1HG0046420*), *Ror1-tail* (*Hv*Myo11A1, *HORVU. MOREX.r3.1HG0046420*; amino acids 879–1509), *Myo11A3-tail* (*HORVU.MOREX.r3.6HG0629580*; amino acids 878–1511 according to the presumed full-length sequence, PCR primers based on Gen-Bank AK368390.1), *Myo11G1-tail* (*HORVU.MOREX.r3.6HG0620190*; amino acids 876–1497 according to the presumed full-length sequence, PCR primers based on GenBank AK363069.1), and *Mlo* (*HORVU.MOREX.r3.4HG0410620*). In all cases, gene expression was driven by the strong constitutive maize *ubiquitin* promoter. Primers used for cloning are listed in Table S4.

Transient gene expression *via* particle bombardment

Transient gene expression *via* particle bombardment was performed using a PDS-1000/He™ Particle Delivery System with Hepta™ Adaptor (Bio-Rad, Feldkirchen, Germany) in combination with GUS staining and *B. hordei* inoculation as described before (Acevedo-Garcia, Spencer, et al., 2017; Panstruga, 2004).

Pharmacological inhibitor experiments

For inhibitor treatments, three or four primary barley leaves were cut off at their base, placed into a 50-mL reaction tube, and overlaid with the respective solution (either water or NEM that was freshly solved in water at the mentioned concentration). Leaves were vacuum-infiltrated in a desiccator for 10 min. At 30 min after release of the vacuum, leaves were placed on agarose plates for an additional hour for regeneration. Thereafter, plates were inoculated with *B. hordei* isolate K1 conidiospores. At 48 hpi, leaves were destained in 80% (v/v) ethanol. The penetration success was determined by staining the fungal structures with 0.6% (w/v) Coomassie in ethanol for 30 sec followed by inspection under a light microscope. The penetration success was calculated as the number of cells harboring at least one haustorium divided by the total number of attacked cells × 100%. At least 50 (typically 200–300) interaction sites were scored per leaf, per experiment three leaves were analyzed, and four independent experiments were performed, resulting in a total of 2000–3200 scored interaction sites per treatment and genotype.

Confocal laser scanning microscopy

For localization of fluorophore-tagged proteins, sections of transiently transformed barley leaves were placed in a droplet of water on a glass slide and shielded with a coverslip. Analyses were performed with a Leica TCS SP8 lightning® confocal microscope and the LAS-X software package (Leica Microsystems, Wetzlar, Germany). Z-stacks were recorded with an HC PL APO CS2 20×/0.75 DRY objective (Leica Microsystems). Fluorescence signals were recorded in sequential scan mode with the following specifications: YFP excitation at 514 nm (argon laser) and emission at 525–555 nm; GFP excitation at 488 nm and emission at 498–515 nm; DsRed and mCherry excitation at 561 nm (DPSS 561 diode) and emission at 570–600 nm. Plasmids pUBI-DsRed-PTS1 and pUBI-GFP-PTS1 express DsRed and GFP variants with a C-terminal peroxisomal-targeting signal (PTS1), while pUBI-mCherry expresses cytosolic mCherry protein. For the analysis of subcellular colocalization of fluorophore-tagged proteins, images were processed using Cell Profiler v4.2.1 (Carpenter et al., 2006), and Manders' overlap coefficient was calculated for determining the degree of colocalization (Manders et al., 1993).

Statistical analysis and graph generation

Statistical analyses and graph (boxplot) generation of data from transient gene expression experiments, localization experiments, and inhibitor treatments were performed using GraphPad Prism v8.4.2 software (GraphPad Prism Software Inc., San Diego, CA, USA). Outliers are indicated by dots. Statistical analyses were performed using one-way or two-way analysis of variance (ANOVA) with either Tukey's or Dunnett's *post hoc* tests to correct for multiple testing.

AUTHOR CONTRIBUTIONS

JA-G performed genomic and transcriptomic analyses and identified *Ror1*. KW performed transient gene expression experiments and protein work. KD helped with mutant verification. MKw, FL, and MF performed confocal microscopy. KB performed initial gene expression experiments. AR performed cloning and transient gene expression experiments. XD, GVJ, MM, NS, LCB, KS, and NB-A conducted bioinformatic analyses. MKo performed phylogenetic analyses and provided myosin expertise. PS-L and RP conceived the study, supervised the work, and wrote the manuscript.

ACKNOWLEDGMENTS

CONFLICT OF INTEREST

The authors declare they have no conflict of interest.

DATA AVAILABILITY STATEMENT

All relevant data except for the *ror* mutant RNA-Seq raw reads can be found within the manuscript and its supporting materials. The RNA-Seq raw reads are stored at NCBI under Bioproject ID PRJNA863083 (https://www.ncbi.nlm. nih.gov/bioproject/PRJNA863083).

SUPPORTING INFORMATION

Additional Supporting Information may be found in the online version of this article.

Figure S1. Gene structures of barley (*H. vulgare*) myosins.

Figure S2. Validation of *ror1* mutant sites by Sanger sequencing.

Figure S3. Haplotype pattern of barley recombinants within the *Ror1* genetic interval.

Figure S4. Sequence conservation within the class XI myosins.

Figure S5. Multiple amino acid sequence alignments of example myosins from the main branches of the eukaryotic tree of life.

Figure S6. Pharmacological inhibitor analysis suggests Ror1 is the only barley myosin involved in *mlo* resistance.

Table S1. Hi-C-based gene order in the *Ror1* interval of barley cv. Morex.

Table S2. Plant material and time points used for RNA-Seq analysis.

Table S3. Number of *Ror1* RNA-Seq reads in various barley samples.

Table S4. Oligonucleotides used in this study.

Data S1. *Ror1* genomic sequence, coding sequence, and deduced amino acid sequence.

Appendix S1. Supporting information.

REFERENCES

Acevedo-Garcia, J., Collins, N.C., Ahmadinejad, N., Ma, L., Houben, A., Bednarek, P. *et al.* (2013) Fine mapping and chromosome walking towards the *Ror1* locus in barley (*Hordeum vulgare* L.). *Theoretical and Applied Genetics*, **126**, 2969–2982.

Acevedo-Garcia, J., Gruner, K., Reinstädler, A., Kemen, A., Kemen, E., Cao, L. *et al.* (2017) The powdery mildew-resistant Arabidopsis *mlo2 mlo6 mlo12* triple mutant displays altered infection phenotypes with diverse types of phytopathogens. *Scientific Reports*, **7**, 27.

Acevedo-Garcia, J., Kusch, S. & Panstruga, R. (2014) Magical mystery tour - MLO proteins in plant immunity and beyond. *The New Phytologist*, **204**, 273–281.

Acevedo-Garcia, J., Spencer, D., Thieron, H., Reinstadler, A., Hammond-Kosack, K., Phillips, A.L. *et al.* (2017) *mlo*-based powdery mildew resistance in hexaploid bread wheat generated by a non-transgenic TILLING approach. *Plant Biotechnology Journal*, **15**, 367–378.

Altschul, S.F., Gish, W., Miller, W., Myers, E.W. & Lipman, D.J. (1990) Basic local alignment search tool. *Journal of Molecular Biology*, **215**, 403–410.

Avisar, D., Abu-Abied, M., Belausov, E., Sadot, E., Hawes, C. & Sparkes, I.A. (2009) A comparative study of the involvement of 17 Arabidopsis myosin family members on the motility of Golgi and other organelles. *Plant Physiology*, **150**, 700–709.

Avisar, D., Prokhnevsky, A.I. & Dolja, V.V. (2008) Class VIII myosins are required for plasmodesmatal localization of a closterovirus Hsp70 homolog. *Journal of Virology*, **82**, 2836–2843.

Bai, Y.L., Pavan, S., Zheng, Z., Zappel, N.F., Reinstädler, A., Lotti, C. *et al.* (2008) Naturally occurring broad-spectrum powdery mildew resistance in a central American tomato accession is caused by loss of *Mlo* function. *Molecular Plant-Microbe Interactions*, **21**, 30–39.

Bednarek, P., Piślewska-Bednarek, M., Svatoš, A., Schneider, B., Doubský, J., Mansurova, M. *et al.* (2009) A glucosinolate metabolism pathway in living plant cells mediates broad-spectrum antifungal defense. *Science*, **323**, 101–106.

Bhat, R.A., Miklis, M., Schmelzer, E., Schulze-Lefert, P. & Panstruga, R. (2005) Recruitment and interaction dynamics of plant penetration resistance components in a plasma membrane microdomain. *Proceedings of the National Academy of Sciences of the United States of America*, **102**, 3135–3140.

Bittins, C.M., Eichler, T.W. & Gerdes, H.-H. (2009) Expression of the dominant-negative tail of myosin Va enhances exocytosis of large dense core vesicles in neurons. *Cellular and Molecular Neurobiology*, **29**, 597–608.

Bloemink, M.J., Melkani, G.C., Bernstein, S.I. & Geeves, M.A. (2016) The relay/converter interface influences hydrolysis of ATP by skeletal muscle myosin II. *The Journal of Biological Chemistry*, **291**, 1763–1773.

Bradford, M.M. (1976) A rapid and sensitive method for the quantitation of microgram quantities of protein utilizing the principle of protein-dye binding. *Analytical Biochemistry*, **72**, 248–254.

Burns, C.G., Larochelle, D.A., Erickson, H., Reedy, M. & de Lozanne, A. (1995) Single-headed myosin II acts as a dominant negative mutation in *Dictyostelium*. *Proceedings of the National Academy of Sciences of the United States of America*, **92**, 8244–8248.

Carpenter, A.E., Jones, T.R., Lamprecht, M.R., Clarke, C., Kang, I.H., Friman, O. *et al.* (2006) CellProfiler: image analysis software for identifying and quantifying cell phenotypes. *Genome Biology*, **7**, R100.

Collins, N.C., Lahaye, T., Peterhänsel, C., Freialdenhoven, A., Corbitt, M. & Schulze-Lefert, P. (2001) Sequence haplotypes revealed by sequence-tagged site fine mapping of the Ror1 gene in the centromeric region of barley chromosome 1H. *Plant Physiology*, **125**, 1236–1247.

Collins, N.C., Thordal-Christensen, H., Lipka, V., Bau, S., Kombrink, E., Qiu, J.L. *et al.* (2003) SNARE-protein-mediated disease resistance at the plant cell wall. *Nature*, **425**, 973–977.

Consonni, C., Humphry, M.E., Hartmann, H.A., Livaja, M., Durner, J., Westphal, L. *et al.* (2006) Conserved requirement for a plant host cell protein in powdery mildew pathogenesis. *Nature Genetics*, **38**, 716–720.

Coureux, P.-D., Sweeney, H.L. & Houdusse, A. (2004) Three myosin V structures delineate essential features of chemo-mechanical transduction. *The EMBO Journal*, **23**, 4527–4537.

de Lanerolle, P. (2012) Nuclear actin and myosins at a glance. *Journal of Cell Science*, **125**, 4945–4949.

DeScenzo, R.A. & Wise, R.P. (1996) Variation in the ratio of physical to genetic distance in intervals adjacent to the *Mla* locus on barley chromosome 1H. *Molecular & General Genetics*, **251**, 472–482.

Devoto, A., Piffanelli, P., Nilsson, I., Wallin, E., Panstruga, R., von Heijne, G. *et al.* (1999) Topology, subcellular localization, and sequence diversity of the Mlo family in plants. *The Journal of Biological Chemistry*, **274**, 34993–35004.

Elliott, C., Müller, J., Miklis, M., Bhat, R.A., Schulze-Lefert, P. & Panstruga, R. (2005) Conserved extracellular cysteine residues and cytoplasmic loop-loop interplay are required for functionality of the heptahelical MLO protein. *The Biochemical Journal*, **385**, 243–254.

Fili, N., Hari-Gupta, Y., dos Santos, Á., Cook, A., Poland, S., Ameer-Beg, S.M. *et al.* (2017) NDP52 activates nuclear myosin VI to enhance RNA polymerase II transcription. *Nature Communications*, **8**, 1871.

Freialdenhoven, A., Peterhänsel, C., Kurth, J., Kreuzaler, F. & Schulze-Lefert, P. (1996) Identification of genes required for the function of non-race-specific *mlo* resistance to powdery mildew in barley. *Plant Cell*, **8**, 5–14.

Fuchs, R., Kopischke, M., Klapprodt, C., Hause, G., Meyer, A.J., Schwarzländer, M. *et al.* (2016) Immobilized subpopulations of leaf epidermal mitochondria mediate PENETRATION2-dependent pathogen entry control in Arabidopsis. *Plant Cell*, **28**, 130–145.

Gao, Q., Wang, C., Xi, Y., Shao, Q., Li, L. & Luan, S. (2022) A receptor–channel trio conducts Ca^{2+} signalling for pollen tube reception. *Nature*, **607**, 534–539.

Glawe, D.A. (2008) The powdery mildews: a review of the world's most familiar (yet poorly known) plant pathogens. *Annual Review of Phytopathology*, **46**, 27–51.

Hématy, K., Lim, M., Cherk, C., Piślewska-Bednarek, M., Sanchez-Rodriguez, C., Stein, M. *et al.* (2020) Moonlighting function of phytochelatin synthase1 in extracellular defense against fungal pathogens. *Plant Physiology*, **182**, 1920–1932.

Hilbert, M., Novero, M., Rovenich, H., Mari, S., Grimm, C., Bonfante, P. *et al.* (2020) *MLO* differentially regulates barley root colonization by beneficial endophytic and mycorrhizal fungi. *Frontiers in Plant Science*, **10**, 9319.

Humphry, M., Consonni, C. & Panstruga, R. (2006) *mlo*-based powdery mildew immunity. Silver bullet or simply non-host resistance? *Molecular Plant Pathology*, **7**, 605–610.

Humphry, M., Reinstädler, A., Ivanov, S., Bisseling, T. & Panstruga, R. (2011) Durable broad-spectrum powdery mildew resistance in pea *er1* plants is conferred by natural loss-of-function mutations in *PsMLO1*. *Molecular Plant Pathology*, **12**, 866–878.

Jacott, C.N., Charpentier, M., Murray, J.D. & Ridout, C.J. (2020) Mildew Locus O facilitates colonization by arbuscular mycorrhizal fungi in angiosperms. *The New Phytologist*, **227**, 343–351.

Jarosch, B., Kogel, K.H. & Schaffrath, U. (1999) The ambivalence of the barley *Mlo* locus: mutations conferring resistance against powdery mildew (*Blumeria graminis* f. sp. *hordei*) enhance susceptibility to the rice blast fungus *Magnaporthe grisea*. *Molecular Plant-Microbe Interactions*, **12**, 508–514.

Jørgensen, J.H. (1992) Discovery, characterization and exploitation of Mlo powdery mildew resistance in barley. *Euphytica*, **63**, 141–152.

Kalyaanamoorthy, S., Minh, B.Q., Wong, T.K.F., von Haeseler, A. & Jermiin, L.S. (2017) ModelFinder: fast model selection for accurate phylogenetic estimates. *Nature Methods*, **14**, 587–589.

Kim, M.C., Panstruga, R., Elliott, C., Müller, J., Devoto, A., Yoon, H.W. *et al.* (2002) Calmodulin interacts with MLO protein to regulate defence against mildew in barley. *Nature*, **416**, 447–450.

Kobayashi, I. & Hakuno, H. (2003) Actin-related defense mechanism to reject penetration attempt by a non-pathogen is maintained in tobacco BY-2 cells. *Planta*, **217**, 340–345.

Kollmar, M. & Mühlhausen, S. (2017) Myosin repertoire expansion coincides with eukaryotic diversification in the Mesoproterozoic era. *BMC Evolutionary Biology*, **17**, 211.

Kronert, W.A., Melkani, G.C., Melkani, A. & Bernstein, S.I. (2014) Mapping interactions between myosin relay and converter domains that power muscle function. *The Journal of Biological Chemistry*, **289**, 12779–12790.

Kusch, S. & Panstruga, R. (2017) *mlo*-based resistance: an apparently universal "weapon" to defeat powdery mildew disease. *Molecular Plant-Microbe Interactions*, **30**, 179–189.

Kwaaitaal, M., Keinath, N.F., Pajonk, S., Biskup, C. & Panstruga, R. (2010) Combined bimolecular fluorescence complementation and förster resonance energy transfer reveals ternary SNARE complex formation in living plant cells. *Plant Physiology*, **152**, 1135–1147.

Kwon, C., Bednarek, P. & Schulze-Lefert, P. (2008) Secretory pathways in plant immune responses. *Plant Physiology*, **147**, 1575–1583.

Langmead, B. & Salzberg, S.L. (2012) Fast gapped-read alignment with Bowtie 2. *Nature Methods*, **9**, 357–359.

Langmead, B., Trapnell, C., Pop, M. & Salzberg, S.L. (2009) Ultrafast and memory-efficient alignment of short DNA sequences to the human genome. *Genome Biology*, **10**, R25.

Li, H., Handsaker, B., Wysoker, A., Fennell, T., Ruan, J., Homer, N. *et al.* (2009) The sequence alignment/map format and SAMtools. *Bioinformatics*, **25**, 2078–2079.

Li, J.-F. & Nebenführ, A. (2007) Organelle targeting of myosin XI is mediated by two globular tail subdomains with separate cargo binding sites. *The Journal of Biological Chemistry*, **282**, 20593–20602.

Lipka, V., Dittgen, J., Bednarek, P., Bhat, R., Wiermer, M., Stein, M. *et al.* (2005) Pre- and postinvasion defenses both contribute to nonhost resistance in *Arabidopsis*. *Science*, **310**, 1180–1183.

Lipka, V. & Panstruga, R. (2005) Dynamic cellular responses in plant-microbe interactions. *Current Opinion in Plant Biology*, **8**, 625–631.

Liu, M., Braun, U., Takamatsu, S., Hambleton, S., Shoukouhi, P., Bisson, K.R. et al. (2021) Taxonomic revision of *Blumeria* based on multi-gene DNA sequences, host preferences and morphology. *Mycoscience*, **62**, 143–165.

Lyngkjær, M.F., Newton, A.C., Atzema, J.L. & Baker, S.J. (2000) The barley *mlo* gene: an important powdery mildew resistance source. *Agronomie*, **20**, 745–756.

Madison, S.L., Buchanan, M.L., Glass, J.D., McClain, T.F., Park, E. & Nebenführ, A. (2015) Class XI myosins move specific organelles in pollen tubes and are required for normal fertility and pollen tube growth in Arabidopsis. *Plant Physiology*, **169**, 1946–1960.

Madison, S.L. & Nebenführ, A. (2013) Understanding myosin functions in plants: are we there yet? *Current Opinion in Plant Biology*, **16**, 710–717.

Malinovsky, F.G., Fangel, J.U. & Willats, W.G.T. (2014) The role of the cell wall in plant immunity. *Frontiers in Plant Science*, **5**, 178.

Manders, E.M.M., Verbeek, F.J. & Aten, J.A. (1993) Measurement of co-localization of objects in dual-colour confocal images. *Journal of Microscopy*, **169**, 375–382.

Mascher, M., Gundlach, H., Himmelbach, A., Beier, S., Twardziok, S.O., Wicker, T. *et al.* (2017) A chromosome conformation capture ordered sequence of the barley genome. *Nature*, **544**, 427–433.

Mascher, M., Wicker, T., Jenkins, J., Plott, C., Lux, T., Koh, C.S. *et al.* (2021) Long-read sequence assembly: a technical evaluation in barley. *The Plant Cell*, **33**, 1888–1906.

McGrann, G.R.D., Stavrinides, A., Russell, J., Corbitt, M.M., Booth, A., Chartrain, L. *et al.* (2014) A trade off between *mlo* resistance to powdery mildew and increased susceptibility of barley to a newly important disease, Ramularia leaf spot. *Journal of Experimental Botany*, **65**, 1025–1037.

Meeusen, R.L. & Cande, W.Z. (1979) *N*-ethylmaleimide-modified heavy meromyosin. A probe for actomyosin interactions. *The Journal of Cell Biology*, **82**, 57–65.

Miklis, M., Consonni, C., Bhat, R.A., Lipka, V., Schulze-Lefert, P. & Panstruga, R. (2007) Barley MLO modulates actin-dependent and actin-independent antifungal defense pathways at the cell periphery. *Plant Physiology*, **144**, 1132–1143.

Moral, J., Montilla-Bascón, G., Canales, F.J., Rubiales, D. & Prats, E. (2017) Cytoskeleton reorganization/disorganization is a key feature of induced inaccessibility for defence to successive pathogen attacks. *Molecular Plant Pathology*, **18**, 662–671.

Mühlhausen, S. & Kollmar, M. (2013) Whole genome duplication events in plant evolution reconstructed and predicted using myosin motor proteins. *BMC Evolutionary Biology*, **13**, 202.

Müller, J., Piffanelli, P., Devoto, A., Miklis, M., Elliott, C., Ortmann, B. *et al.* (2005) Conserved ERAD-like quality control of a plant polytopic membrane protein. *Plant Cell*, **17**, 149–163.

Nebenführ, A. & Dixit, R. (2018) Kinesins and myosins: molecular motors that coordinate cellular functions in plants. *Annual Review of Plant Biology*, **69**, 329–361.

Nguyen, L.-T., Schmidt, H.A., von Haeseler, A. & Minh, B.Q. (2015) IQ-TREE: a fast and effective stochastic algorithm for estimating maximum-likelihood phylogenies. *Molecular Biology and Evolution*, **32**, 268–274.

Odronitz, F. & Kollmar, M. (2007) Drawing the tree of eukaryotic life based on the analysis of 2,269 manually annotated myosins from 328 species. *Genome Biology*, **8**, R196.

Opalski, K.S., Schultheiss, H., Kogel, K.H. & Hückelhoven, R. (2005) The receptor-like MLO protein and the RAC/ROP family G-protein RACB modulate actin reorganization in barley attacked by the biotrophic powdery mildew fungus Blumeria graminis f.sp. hordei. *The Plant Journal*, **41**, 291–303.

Panstruga, R. (2004) A golden shot: How ballistic single cell transformation boosts the molecular analysis of cereal-mildew interactions. *Molecular Plant Pathology*, **5**, 141–148.

Park, E., Nedo, A., Caplan, J.L. & Dinesh-Kumar, S.P. (2018) Plant-microbe interactions: organelles and the cytoskeleton in action. *The New Phytologist*, **217**, 1012–1028.

Peremyslov, V.V., Klocko, A.L., Fowler, J.E. & Dolja, V.V. (2012) *Arabidopsis* myosin XI-K localizes to the motile endomembrane vesicles associated with F-actin. *Frontiers in Plant Science*, **3**, 184.

Peremyslov, V.V., Mockler, T.C., Filichkin, S.A., Fox, S.E., Jaiswal, P., Makarova, K.S. *et al.* (2011) Expression, splicing, and evolution of the myosin gene family in plants. *Plant Physiology*, **155**, 1191–1204.

Peremyslov, V.V., Prokhnevsky, A.I., Avisar, D. & Dolja, V.V. (2008) Two class XI myosins function in organelle trafficking and root hair development in Arabidopsis. *Plant Physiology*, **146**, 1109–1116.

Peterhänsel, C., Freialdenhoven, A., Kurth, J., Kolsch, R. & Schulze-Lefert, P. (1997) Interaction analyses of genes required for resistance responses to powdery mildew in barley reveal distinct pathways leading to leaf cell death. *Plant Cell*, **9**, 1397–1409.

Piffanelli, P., Zhou, F.S., Casais, C., Orme, J., Jarosch, B., Schaffrath, U. *et al.* (2002) The barley MLO modulator of defense and cell death is responsive to biotic and abiotic stress stimuli. *Plant Physiology*, **129**, 1076–1085.

Radford, J.E. & White, R.G. (2011) Inhibitors of myosin, but not actin, alter transport through Tradescantia plasmodesmata. *Protoplasma*, **248**, 205–216.

Ramanath, S., Wang, Q., Bernstein, S.I. & Swank, D.M. (2011) Disrupting the myosin converter-relay interface impairs *Drosophila* indirect flight muscle performance. *Biophysical Journal*, **101**, 1114–1122.

Reichelt, S., Knight, A.E., Hodge, T.P., Baluska, F., Samaj, J., Volkmann, D. *et al.* (1999) Characterization of the unconventional myosin VIII in plant cells and its localization at the post-cytokinetic cell wall. *The Plant Journal*, **19**, 555–567.

Reinstädler, A., Müller, J., Czembor, J.H., Piffanelli, P. & Panstruga, R. (2010) Novel induced *mlo* mutant alleles in combination with site-directed mutagenesis reveal functionally important domains in the heptahelical barley Mlo protein. *BMC Plant Biology*, **10**, 31.

Robert-Paganin, J., Pylypenko, O., Kikuti, C., Sweeney, H.L. & Houdusse, A. (2020) Force generation by myosin motors: a structural perspective. *Chemical Reviews*, **120**, 5–35.

Ryan, J.M. & Nebenführ, A. (2018) Update on myosin motors: molecular mechanisms and physiological functions. *Plant Physiology*, **176**, 119–127.

Sattarzadeh, A., Schmelzer, E. & Hanson, M.R. (2011) Analysis of organelle targeting by DIL domains of the Arabidopsis myosin XI family. *Frontiers in Plant Science*, **2**, 72.

Schmelzer, E. (2002) Cell polarization, a crucial process in fungal defence. *Trends in Plant Science*, **7**, 411–415.

Sparkes, I. (2011) Recent advances in understanding plant myosin function: life in the fast lane. *Molecular Plant*, **4**, 805–812.

Stephan, L., Jakoby, M., Das, A., Koebke, E. & Hülskamp, M. (2021) Unravelling the molecular basis of the dominant negative effect of myosin XI tails on P-bodies. *PLoS One*, **16**, e0252327.

Stephens, J.L., Brown, S.E., Lapitan, N.L.V. & Knudson, D.L. (2004) Physical mapping of barley genes using an ultrasensitive fluorescence in situ hybridization technique. *Genome*, **47**, 179–189.

Takemoto, D., Jones, D.A. & Hardham, A.R. (2003) GFP-tagging of cell components reveals the dynamics of subcellular re-organization in response to infection of Arabidopsis by oomycete pathogens. *The Plant Journal*, **33**, 775–792.

Tamura, K., Iwabuchi, K., Fukao, Y., Kondo, M., Okamoto, K., Ueda, H. *et al.* (2013) Myosin XI-i links the nuclear membrane to the cytoskeleton to control nuclear movement and shape in *Arabidopsis*. *Current Biology*, **23**, 1776–1781.

Thomas, M., Huck, N., Hoehenwarter, W., Conrath, U. & Beckers, G.J.M. (2015) Combining metabolic ^{15}N labeling with improved tandem MOAC for enhanced probing of the phosphoproteome. In: Schulze, W.X. (Ed.) *Plant Phosphoproteomics*. New York, NY: Springer New York, pp. 81–96.

Thorvaldsdóttir, H., Robinson, J.T. & Mesirov, J.P. (2013) Integrative Genomics Viewer (IGV). High-performance genomics data visualization and exploration. *Briefings in Bioinformatics*, **14**, 178–192.

Tominaga, M., Kojima, H., Yokota, E., Orii, H., Nakamori, R., Katayama, E. *et al.* (2003) Higher plant myosin XI moves processively on actin with 35 nm steps at high velocity. *The EMBO Journal*, **22**, 1263–1272.

Tominaga, M. & Nakano, A. (2012) Plant-specific myosin XI, a molecular perspective. *Frontiers in Plant Science*, **3**, 211.

Trapnell, C., Pachter, L. & Salzberg, S.L. (2009) TopHat: discovering splice junctions with RNA-Seq. *Bioinformatics*, **25**, 1105–1111.

Venit, T., Semesta, K., Farrukh, S., Endara-Coll, M., Havalda, R., Hozak, P. *et al.* (2020) Nuclear myosin 1 activates p21 gene transcription in response to DNA damage through a chromatin-based mechanism. *Communications Biology*, **3**, 115.

Wang, Y., Cheng, X., Shan, Q., Zhang, Y., Liu, J., Gao, C. *et al.* (2014) Simultaneous editing of three homoeoalleles in hexaploid bread wheat confers heritable resistance to powdery mildew. *Nature Biotechnology*, **32**, 947–951.

Wu, S.-Z. & Bezanilla, M. (2014) Myosin VIII associates with microtubule ends and together with actin plays a role in guiding plant cell division. *eLife*, **3**, e03498.

Yang, L., Qin, L., Liu, G., Peremyslov, V.V., Dolja, V.V. & Wei, Y. (2014) Myosins XI modulate host cellular responses and penetration resistance to fungal pathogens. *Proceedings of the National Academy of Sciences of the United States of America*, **111**, 13996–14001.